ESD-TDR-65-458

Technical Report 404

B. F. LaPage

Lincoln Experimental Terminal Antenna System

4 October 1965

Prepared under Electronic Systems Division Contract AF 19(628)-5167 by

Lincoln Laboratory
MASSACHUSETTS INSTITUTE OF TECHNOLOGY
Lexington, Massachusetts

The work reported in this document was performed at Lincoln Laboratory, a center for research operated by Massachusetts Institute of Technology, with the support of the U.S. Air Force under Contract AF 19(628)-5167.

Distribution of this document is unlimited.

MASSACHUSETTS INSTITUTE OF TECHNOLOGY

LINCOLN LABORATORY

LINCOLN EXPERIMENTAL TERMINAL ANTENNA SYSTEM

B. F. LaPAGE

Group 61

TECHNICAL REPORT 404

4 OCTOBER 1965

LEXINGTON MASSACHUSETTS

ABSTRACT

The Lincoln Experimental Terminal (LET) is a small transportable ground terminal for testing and evaluating space communications techniques. The requirements, design analysis, and performance data for the LET antenna and feed system are described. The 15-foot-aperture antenna has Cassegrainian optics, and a conical-horn-reflector feed exciter producing opposite-hand circularly polarized transmitting and receiving beams. The simultaneous operation of a two-channel tracking system is also discussed.

Accepted for the Air Force
Franklin C. Hudson
Chief, Lincoln Laboratory Office

CONTENTS

LINCOLN EXPERIMENTAL TERMINAL ANTENNA SYSTEM

I. INTRODUCTION

The Lincoln Experimental Terminal (LET) is a small transportable ground terminal for testing and evaluating space communications techniques. This report will discuss the requirements, design, and performance of the LET antenna and feed system. Table I lists some of the antenna system requirements.

The LET antenna is a 15-foot-diameter paraboloid with an f/D ratio of 0.312. A Cassegrainian system is used with a 22-inch-diameter hyperboloidal subreflector held in position by four $1\frac{1}{2}$-inch-diameter tubular aluminum spars. The subreflector can be manually positioned along and normal to the focal axis to allow focusing. The rms deviation of the antenna surface from a true paraboloid is only 0.013 inch (0.01λ), and there is no measurable change in the total rms surface deviation when the antenna is disassembled and reassembled.* The geometry of the antenna is shown in Fig. 1, along with the general feed-horn configuration. The input ports shown will be designated herein as receive sum (REC-Σ), transmit sum (TX-Σ), and tracking port (Δ).

Since the physical configuration of the LET antenna mount requires that the feed input be stationary and on the elevation axis, the feed system must include a radiating aperture, a right-angle bend, and a rotary joint; a low-loss transmission path is also desirable. The feed horn known as a conical-horn reflector[1] provides a satisfactory solution to this problem. The conical horn reflector uses a section of a paraboloid to transform, approximately, a spherical wave in circular tapered waveguide to a plane wave in circular waveguide, with a 90° change in propagation direction. The circular waveguide radiates from its open end, illuminating the subreflector, and is the actual feed horn in this system. The conical-horn reflector is also suitable in this application, since it will perform equally well with either of two orthogonal linearly polarized signals and hence the required circular polarization. A rotary joint is used in the feed-horn assembly to allow relative motion of the antenna in the elevation plane. The complete feed system is shown in Fig. 2. Figures 3 (a-b) show the antenna and vehicle, and also the antenna as mounted for pattern measurements. The twelve surface segments and radial trusses can be seen along with the removable boom and subreflector assembly.

*Measured at the manufactuer's plant, Advanced Structures, Division of Whittaker Corporation, La Mesa, California.

TABLE I LET ANTENNA SYSTEM REQUIREMENTS	
Antenna gain (8.0 GHz)	48.7 db
Half-power beamwidth (8.0 GHz)	0.58°
Operating band	7.2 to 8.4 GHz
Dynamic bandwidth	±10 MHz
Transmitting polarization	RHCP*
Receiving and tracking polarizations	LHCP
Isolation (TX-Σ to REC-Σ)	⩾20 db
Axial ratio	⩽3 db
Receiver noise temperature	≈100°K
Power capability	25 kw CW

*RHCP right-hand circular polarization; LHCP, left-hand circular polarization.

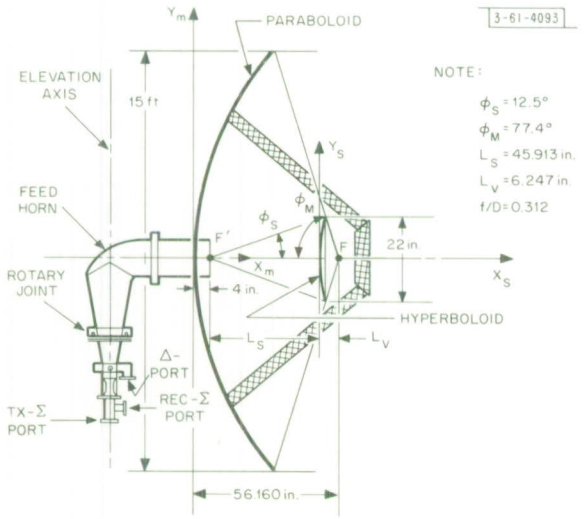

Fig. 1. Antenna geometry.

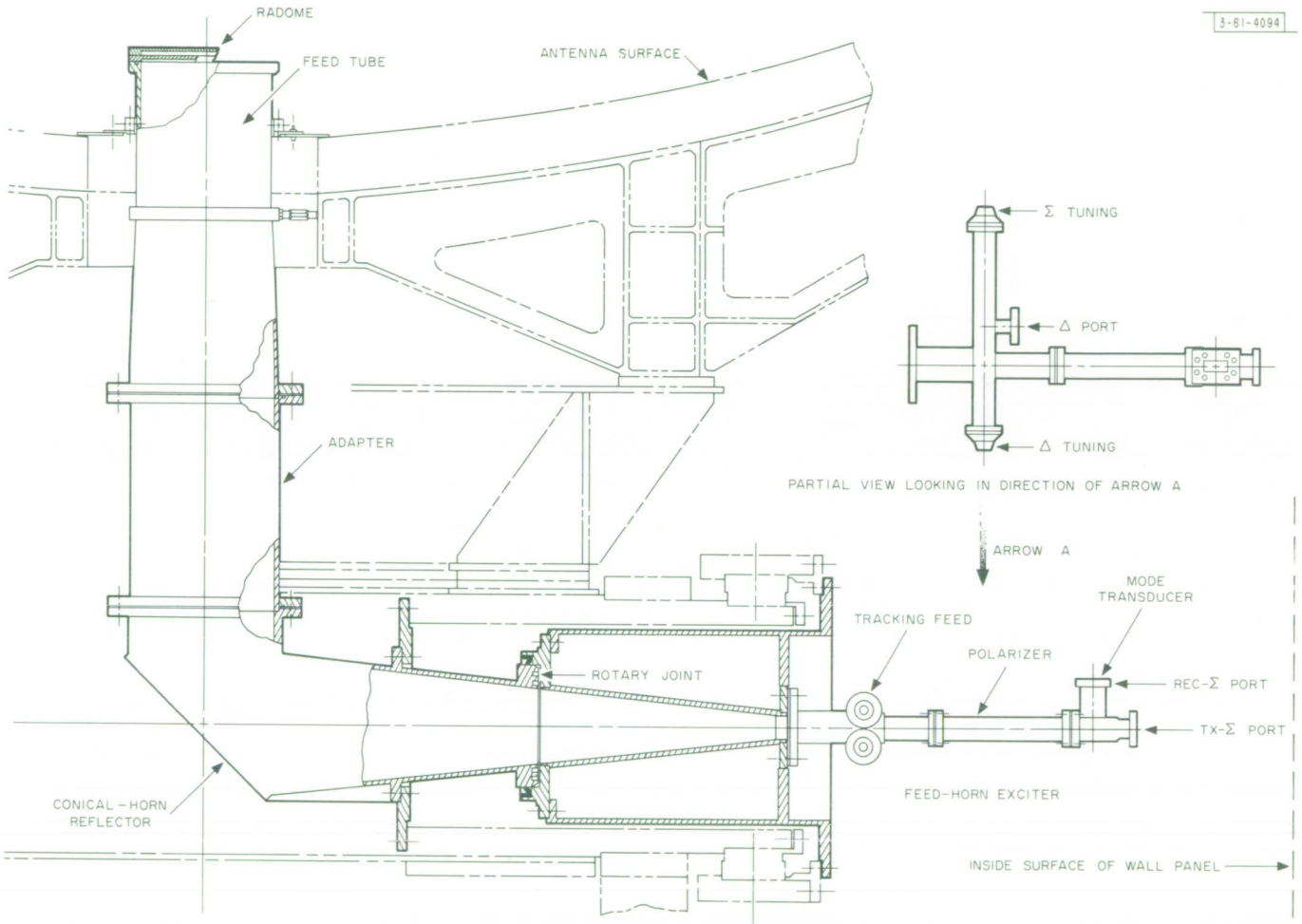

Fig. 2. Antenna feed system.

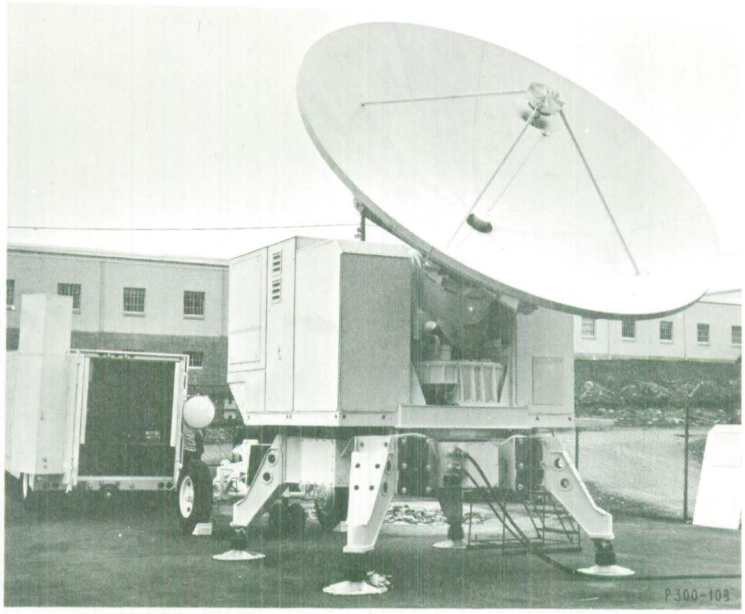

(a) Antenna and vehicle.

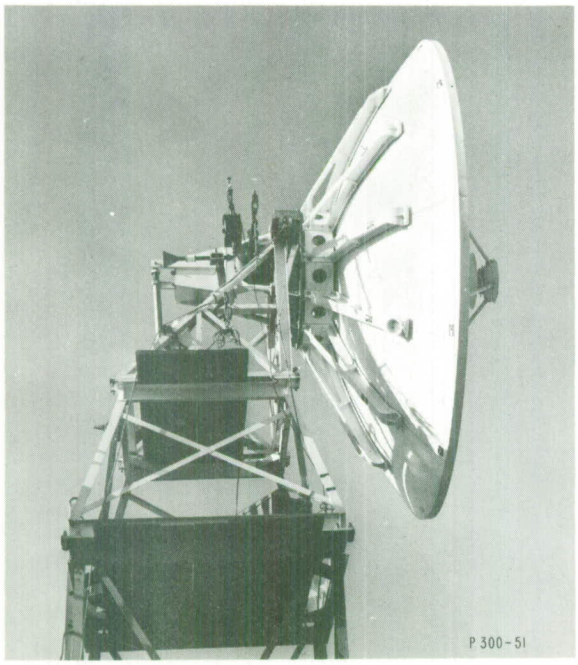

(b) Antenna on test mount.

Fig. 3. The Antenna.

II. FEED-HORN EXCITER

A. Introduction

The feed-horn exciter is shown in Figs. 4(a-b) and also in Fig. 2. The various components have the following functions:

> Mode Transducer – The orthogonal-mode transducer (OMT) produces two orthogonal linearly polarized signals that excite the polarizer unit. It has input ports labeled TX-Σ and REC-Σ.
>
> Polarizer – The polarizer produces a circularly polarized wave from a linearly polarized incident wave.
>
> Tracking Unit – The tracking unit produces, at its output port (Δ), a signal that has a distribution in the feed-horn aperture which will give far-field patterns of a "difference" nature suitable for the generation of a tracking error signal. The tracking unit must also operate with minimal disturbance of the mode transducer and polarizer functions.

These components will now be discussed in greater detail.

B. Orthogonal-Mode Transducer Unit

The choice of the output waveguide dimensions of the OMT is dictated by the required operating bandwidth and the transition to the polarizer unit. One needs to make the output large enough to propagate the rectangular waveguide TE_{10} mode from 7.2 to 8.4 GHz, but not so large that higher-order modes might be a problem. Also, increasing the size of the square waveguide which carries the dual polarized waves reduces the overall length of the polarizer. Square waveguide cutoff characteristics are shown in Fig. 5. The final compromise was a waveguide size of 1.000 inch square. Input ports of the OMT consist of WR-112 waveguide with CPR-112 flanges. Figures 2, 4(a-b), and 6 show the final unit. Overall unit length was restricted to less than four inches to accommodate the distance between the input terminal of the feed and the equipment in the shelter. A two-section quarter-wave transformer was used in the TX-Σ arm of the OMT to match the unit over the required band. Inductive irises and mode-suppressing fins are used to match the REC-Σ arm. Final input admittance data are given in Figs. 7(a-b). Input VSWR is less than 1.18:1 over the 7.4 to 8.4-GHz band. The OMT was matched in this fashion, since operation at 7.2 GHz would be infrequent, if at all, and it was planned to use external matching devices as required to improve the performance in this band. Isolation between TX-Σ and REC-Σ ports, with the output port terminated in a matched load, is given in Fig. 8. Although this isolation is very good, it should be kept in mind that the isolation of these ports in the complete system will depend mostly on reflections from the tracking unit, radome, and subreflector. The OMT and other units in the exciter assembly were electroformed of oxygen-free high-conductivity (OFHC) copper, using polished aluminum mandrels. A dimensional accuracy of ±0.002 inch and a surface finish of 16 μ inches was readily obtained by this technique.

C. Polarizer Unit

Polarizer design is based on some of the author's previous work[2] and on the published data of Assaly[3] and Kessler.[4] The polarizer produces a circularly polarized wave from a linearly polarized input due to the differential phase shift caused by the wedge loading of a square waveguide. Figure 9 shows the final unit and Fig. 10 shows the axial ratio of the circularly polarized

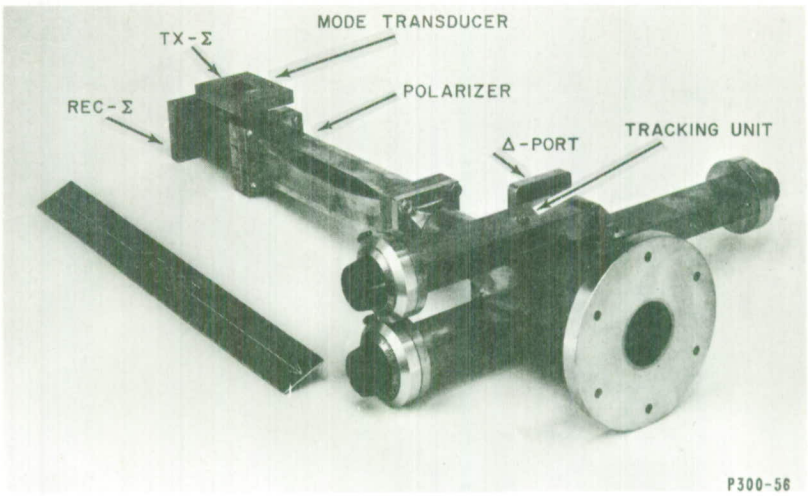

(a) Front.

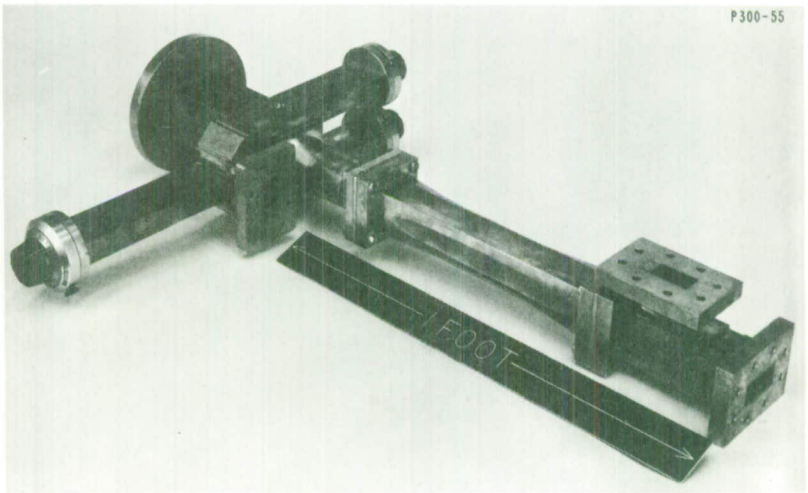

(b) Rear.

Fig. 4. Feed-horn exciter unit.

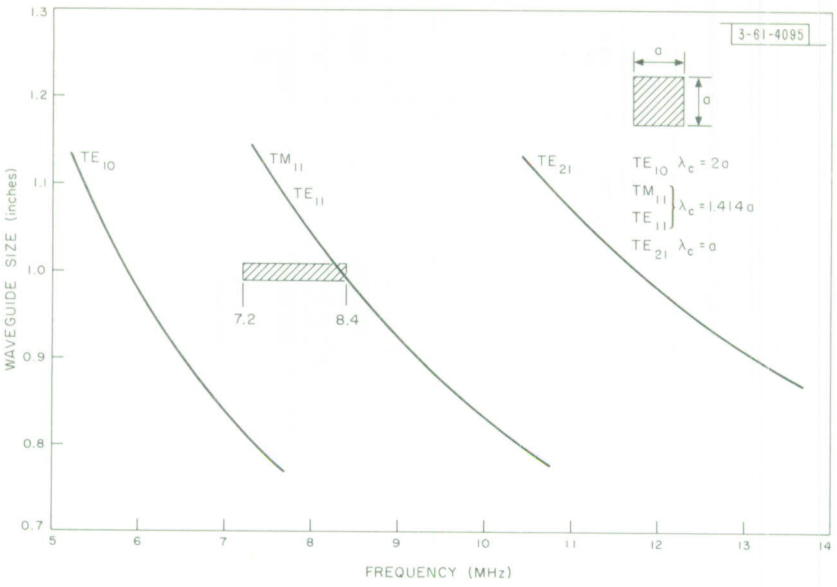

Fig. 5. Cutoff dimensions for square waveguide modes.

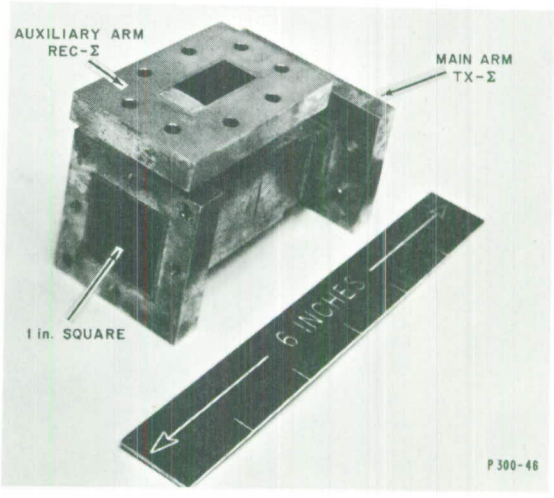

Fig. 6. Orthogonal mode transducer (OMT).

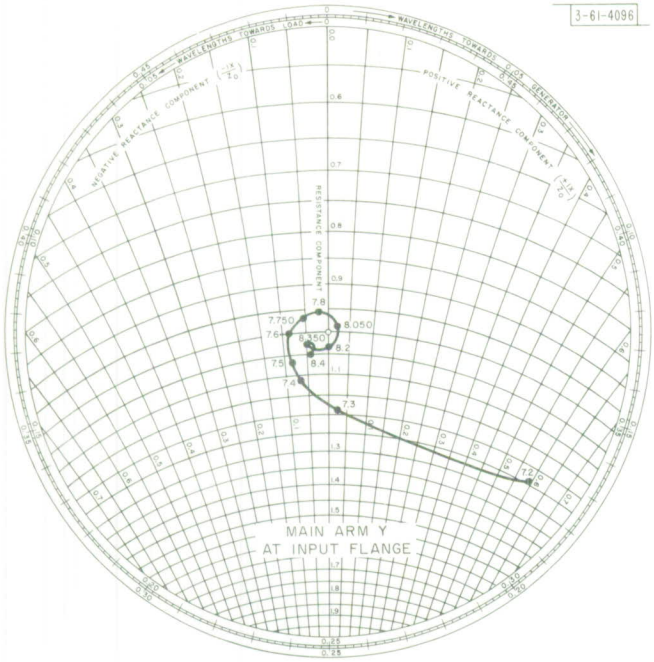

(a) TX-Σ port.

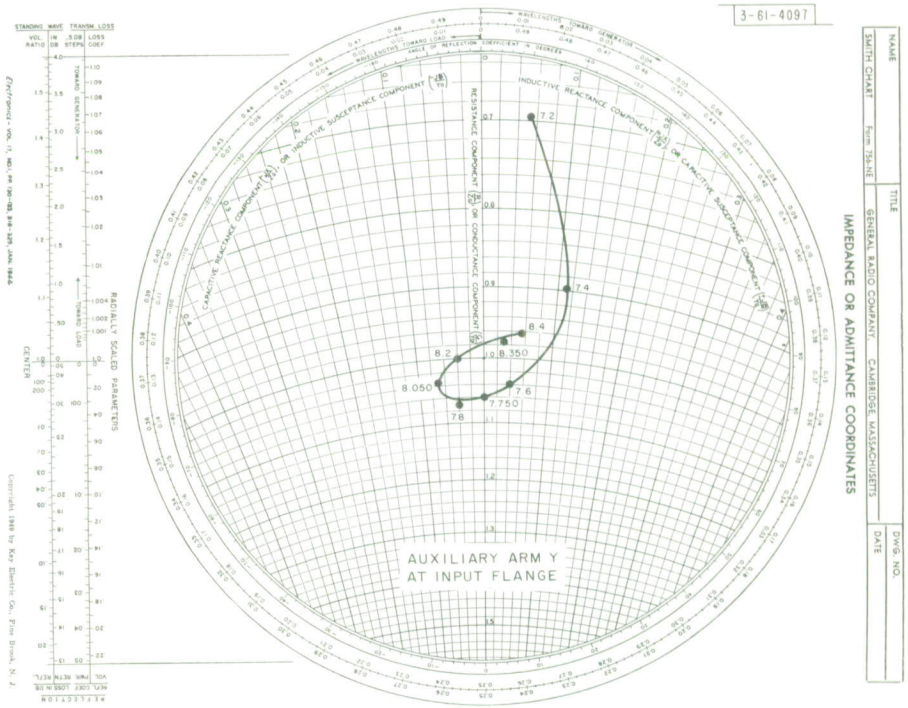

(b) REC-Σ port.

Fig. 7. Input admittance.

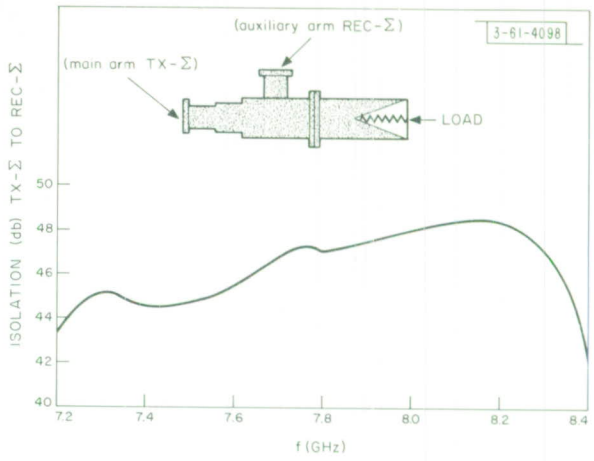

Fig. 8. Isolation of OMT (TX-Σ to REC-Σ ports).

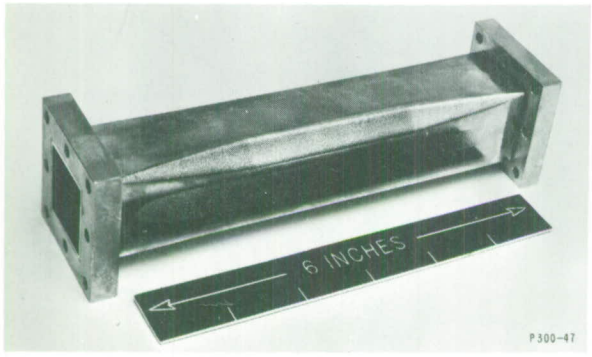

Fig. 9. Polarizer unit.

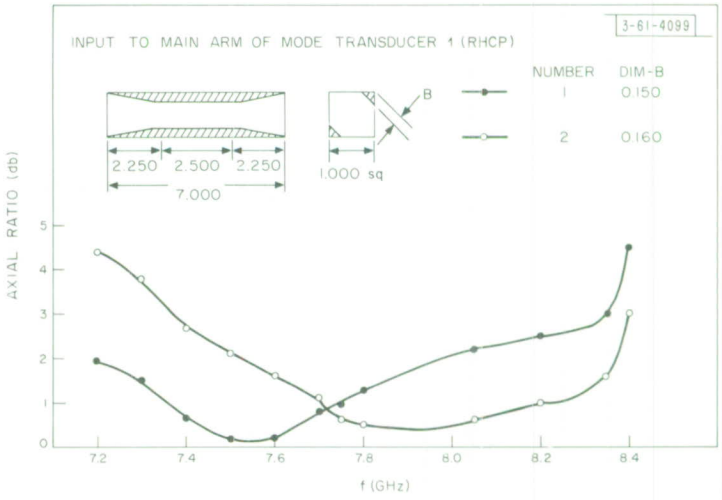

Fig. 10. Axial ratio of polarizer units.

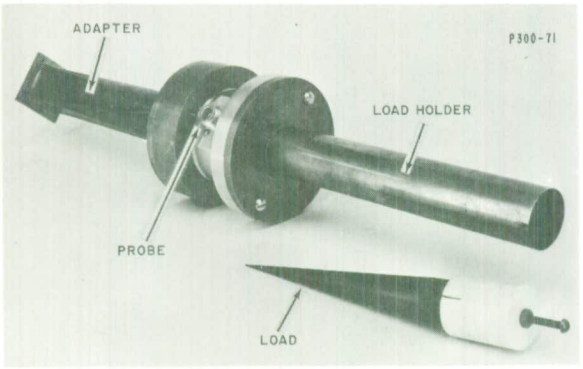

Fig. 11. Polarization analyzer.

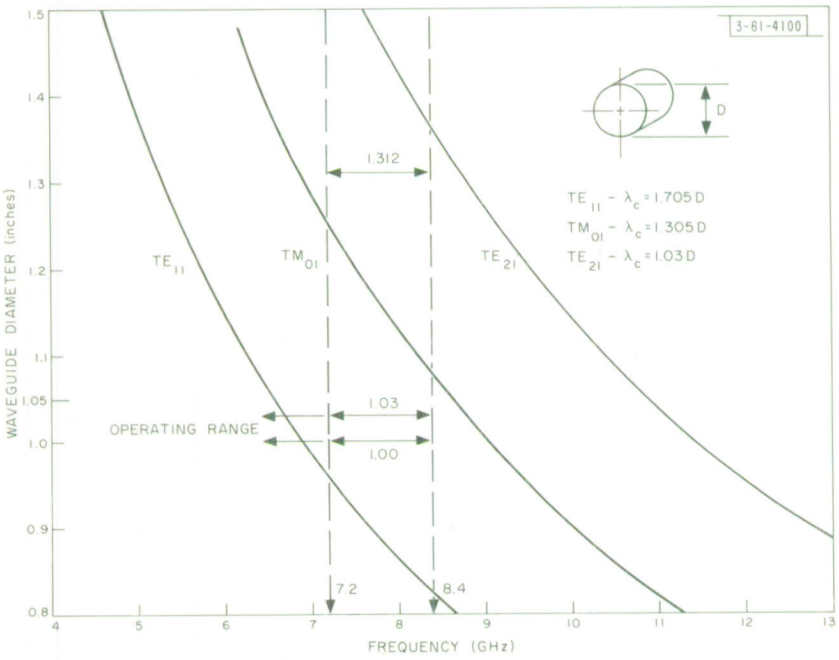

Fig. 12. Cutoff dimensions for circular waveguide modes.

wave produced by the polarizer. Pertinent dimensions are given for two models and it can be seen that a change of only 0.010 inch in the wedge depth produces a significant change in the polarizer characteristics. Since the polarizer is a relatively easy unit to replace in the feed system, two units were supplied to cover the full 7.2- to 8.4-GHz band. Orientation of the polarizer wedges relative to the mode transducer is such that the TX-Σ port radiates RHCP from the antenna.

Polarizer axial ratio was measured by using the polarization analyzer shown in Fig. 11. This device samples the radial component of the electric field in the circular waveguide. Moving the sampling probe circumferentially produces a maximum and a minimum signal that determines the axial ratio of the wave propagating in the circular waveguide. Very low reflection transitions from square to circular waveguide and a sliding load complete the analyzer assembly.

D. Tracking Unit

The tracking unit is essentially a selective mode device that couples to the TM_{01} mode in circular waveguide, while not affecting the circularly polarized TE_{11} mode produced by the mode transducer-polarizer unit. The cutoff sizes for the lowest-order modes in circular waveguide are shown in Fig. 12. A waveguide diameter of 1.312 inches was chosen to allow propagation of both the TM_{01} and TE_{11} modes over the 7.2- to 8.4-GHz band. Moreover, a circular waveguide diameter of 1.03 inches will allow the TE_{11} mode to propagate, while cutting off the TM_{01} mode. This property of the 1.03-inch waveguide is used along with a single quarter-wave transformer to help match the mode coupler. Figure 13 shows these details in a simplified drawing. The field in the circular waveguide is coupled to the two waveguide arms through coupling holes; performance is optimized by adjusting the tuning posts, the position of the TM_{01} cutoff section, and the two short-circuiting plungers in the waveguide arms. The signals are then combined

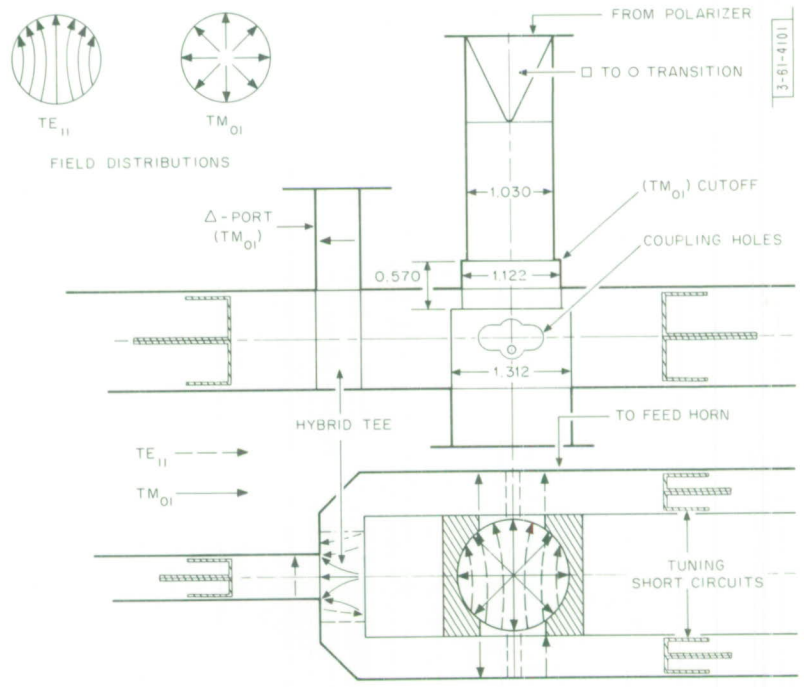

Fig. 13. Tracking unit schematic.

TABLE II

FEED-HORN EXCITER TUNING DATA

(Measurements made in vehicle directly on ports of tracking feed.)

Port	Frequency (MHz)	VSWR	Frequency (MHz)	Isolation (db) TX-Σ to Port
Transmit, F_2; Receive, F_1				
Settings: Short Circuits 1 and 2, 7.50; Short Circuit 3, 1.76				
TX-Σ	$F_2 - 10$	1.11		
	F_2	1.04		
	$F_2 + 10$	1.09		
REC-Σ	$F_1 - 10$	1.07	$F_2 - 10$	21.8
	F_1	1.06	F_2	27.0
	$F_1 + 10$	1.08	$F_2 + 10$	33.7
Δ	$F_1 - 10$	1.29	$F_2 - 10$	26.9
	F_1	1.34	F_2	28.5
	$F_1 + 10$	1.37	$F_2 + 10$	28.0
Transmit, F_1; Receive, F_2				
Settings: Short Circuits 1 and 2, 9.95; Short Circuit 3, 11.70				
TX-Σ	$F_1 - 10$	1.11		
	F_1	1.14		
	$F_1 + 10$	1.15		
REC-Σ	$F_2 - 10$	1.07	$F_1 - 10$	18.0
	F_2	1.04	F_1	19.0
	$F_2 + 10$	1.06	$F_1 + 10$	21.7
Δ	$F_2 - 10$	1.40	$F_1 - 10$	34.5
	F_2	1.36	F_1	32.3
	$F_2 + 10$	1.15	$F_1 + 10$	30.2

in a hybrid tee. Because of the symmetry of the hybrid, the signal out of the sum arm of the hybrid comes from the TM_{01} mode and the signal out of the difference arm comes from the TE_{11} mode. By placing a short-circuiting plunger in the TE_{11} mode arm of the hybrid, we can minimize the TE_{11} coupled signal without adversely affecting the TM_{01} coupling. The TE_{11} mode loss can be quite low, a typical value is 0.10 db or less. The coupling holes and matching adjustments were varied experimentally, and by using a swept-frequency display of attenuation and reflection coefficient on an oscilloscope, it was possible to achieve an operating bandwidth of ±10 MHz for the coupler. Tuning over the 7.2- to 8.4-GHz band is accomplished by the use of the movable short-circuiting plungers in the three waveguide arms. The final tracking unit is shown in Figs. 4(a-b). Helipot (Helipot Division of Beckman Instruments, Inc.) dials were used as short-circuit position indicators because they are physically compact, easy to read at an angle, and they provide a positive locking device. Since there is some interaction and tradeoff possible in the tuning procedure, it is necessary to know the specific transmitting and receiving frequencies to be used. The only combinations of frequencies known at the time of adjustment are those given in Table II, with the measured characteristics of the tracking unit installed in the antenna. Measured insertion loss of the unit was TE_{11} − 0.07 db, TM_{01} − 0.25 db. This was measured by placing the tracking unit and a prototype model back to back and taking one-half the total loss as that due to the final tracking unit. Tuning adjustments were also checked to ensure that the full operating bandwidth could be covered. The tracking unit can be tuned to any required set of frequencies without removing it from the feed system.

The tracking function is accomplished by utilizing the signals from the Δ-port and the REC-Σ port [Figs. 1, 2, and 4(a-b)]. Secondary antenna patterns produced by excitation of these ports are shown in Figs. 14(a-d). The Δ-port patterns are shown with only the Σ-port polarization,

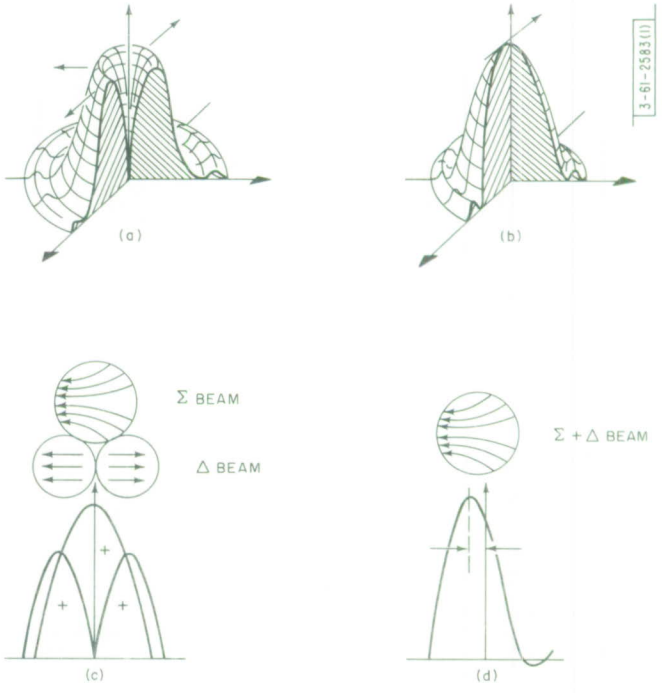

Fig. 14. Tracking patterns.
(a) Pattern at Δ-port.
(b) Pattern at REC-Σ port.
(c) Sum and error pattern.
(d) Total tracking pattern.

the cross-polarized components which exist are not shown. By adding the Σ and Δ patterns [Fig. 14(c)], we obtain the total tracking pattern shown in Fig. 14(d). The plane of the displaced beam is a function of the relative phase shift between the Σ and Δ patterns, and by using fixed 90° phase shifts we can get antenna beam displacements in the elevation and azimuth planes. As presently designed, this tracking circuit will function properly only when receiving left-hand circularly polarized signals, since the Σ-port will respond properly only to this signal polarization. For a linearly polarized signal, an error response will occur only in the plane of polarization and not in the orthogonal plane. A complete discussion of a similar system has been given by Cook, et al.,[5] and will not be given here.

Since the tracking exciter is fixed while the antenna moves in the elevation plane, the tracking-error coordinate system must rotate in elevation with the antenna motion. To compensate for this motion, an angle correction must be supplied to the error signals to indicate the true pointing angle. This is done in the servo system of the antenna, using sine-cosine resolvers.

E. Rotary Joint

The rotary joint consists of a dual quarter-wave choke located a quarter wavelength from the circular waveguide inner wall (Fig. 2). Since the choke groove and connecting parallel-plate transmission line operate essentially in a TEM mode, when excited by either the TE_{11} or TM_{01} mode, the operation is identical. The VSWR in the main waveguide caused by the rotary joint discontinuity is estimated to be about 1.015:1 over the 7.2- to 8.4-GHz band. This value is inferred from measurements of a single choke groove in which the spacing of several small discontinuities such as loads and tapers was varied to produce maximum and minimum VSWR values.

III. FEED HORN AND ANTENNA DESIGN AND PERFORMANCE

A. Antenna Geometry

The antenna geometry (Fig. 1) was chosen to satisfy many requirements, not all of which were under the antenna designer's control. The antenna diameter was chosen to give the maximum gain possible within the limitations of an acceptable structure. The focal length was chosen to accommodate a realistic mechanical structure and those values generally available from prospective vendors. One would like to keep the subreflector as small as possible to minimize the aperture blockage, but this makes the included angle to the subreflector small, requiring a larger feed-horn aperture for proper illumination, which may in turn increase the aperture blockage. The usual compromise is to make the subreflector and feed-horn aperture approximately equal. An additional constraint, which further limits the choice of geometry, is that the subreflector should be in the far field of the feed horn. This ensures that the subreflector is illuminated by a spherical wave emanating from the feed-horn phase center, a basic requirement of the Cassegrainian geometry. A subreflector diameter of 22 inches was chosen after computing several trial designs. The supporting booms cause additional blockage and a boom diameter of $1\frac{1}{2}$ inches was chosen as the minimum size that would keep the subreflector accurately positioned during operation of the antenna.

B. Conical-Horn-Reflector Characteristics

The geometry of the conical-horn reflector is shown in Figs. 15(a-b). It has been shown by Hines, et al.,[1] that this geometry transforms a polar coordinate system in the cone to a bipolar system in the horn aperture. This transformation destroys the polar symmetry by crowding the coordinate lines closer to the cone vertex. Another way of looking at this effect is to note that because of the different space attenuation of the fields in the cone-paraboloid region, there is an amplitude (not phase) taper across the horn aperture in the plane of the cone axis (longitudinal plane). The symmetry of the field, however, is still maintained in the orthogonal plane (transverse plane). This amplitude taper excites higher-order modes and the combined effect is the distortion of the fields as shown in Fig. 15(b). One would expect that as the cone angle is reduced, the distortion of the fields would decrease and the fields would approach those of uniform waveguide modes. In this feed horn, the cone half-angle is about 6° and the conical-horn patterns are very close to the open-ended waveguide patterns, especially to the 10-db points. It will be shown later that this part of the feed-horn pattern is all that is needed, along with the measured feed-horn gain, to calculate the overall antenna efficiency. Hines, et al.,[1] give the conical-horn-reflector gain, for a cone half-angle of about 16°, as $0.806\ (ka)^2$, whereas the TE_{11} mode waveguide radiator gain is $0.837\ (ka)^2$ (Appendix A). This is a gain difference of only 0.155 db in this case, and consequently much less difference in our case, because of the smaller cone angle. Because we shall use mostly the measured gain and patterns in our computations, the relatively simple open-ended waveguide field expressions will be used instead of the more-exact conical-horn-reflector field.

C. Antenna Efficiency and Pattern Calculations

Having chosen the antenna geometry and feed horn, it remains to determine the optimum feed-horn aperture that will maximize the antenna gain. To show the relationship between the feed-horn aperture and the antenna gain, we must develop some geometric properties of the Cassegrainian system (Fig. 16). With the usual approximations of geometric optics, we may apply the concept of the equivalent parabola.[6] It is shown in Appendix B that we can then write for the antenna efficiency η

$$\eta = \frac{\cot^2(\gamma_o/2)}{4\pi^2}\, G_f \left| \int_o^{2\pi} \int_o^{\gamma_o} E(\gamma, \xi) \tan\frac{\gamma}{2}\, d\gamma\, d\xi \right|^2 \qquad (1)$$

where $E(\gamma, \xi)$ is the normalized feed-horn voltage pattern, G_f is the feed-horn on-axis power gain, and η is defined as the antenna efficiency by the usual expression $G = (\pi D/\lambda)^2\, \eta$, where G is the antenna gain and D the main reflector diameter. This expression is well suited to the use of experimental data, with G_f the measured feed-horn gain and $E(\gamma, \xi)$ the average of the E- and H-plane measured feed-horn patterns. It should be noted that only that portion of the feed-horn pattern subtended by the angle $\pm\gamma_o$ is significant in Eq. (1). We have adopted the approach of using the theoretical calculations as a design guide and also using the measured feed-horn data to determine the optimum aperture size.

The fields radiated by an open-ended circular waveguide in the TE_{11} and TM_{01} modes and all subsequent formulas are derived in the Appendices and only the results are repeated here. For the X- and Y-components of the field in the feed-horn aperture, we have[7]

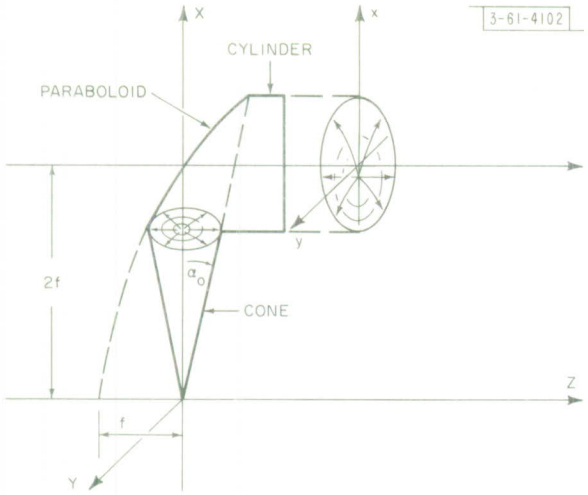

Fig. 15(a). Conical-horn-reflector geometry.

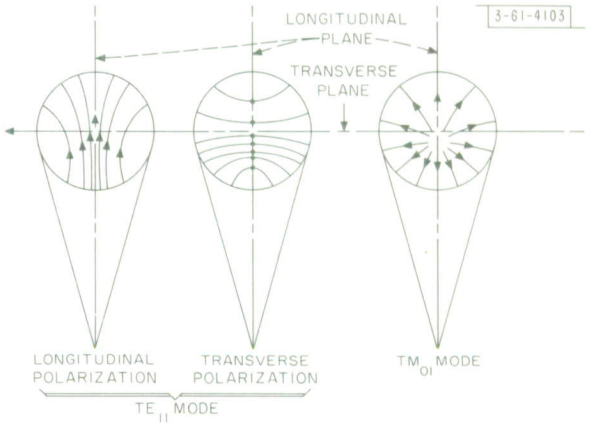

Fig. 15(b). Distortion of field lines.

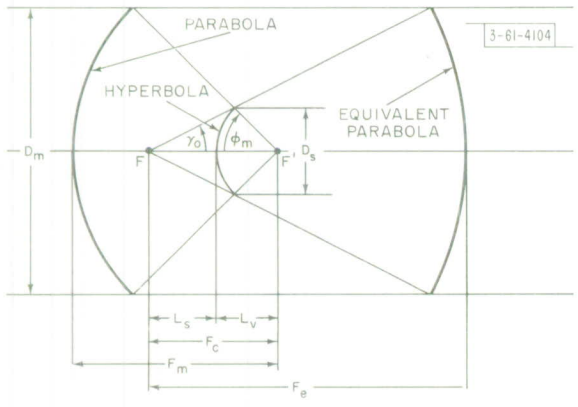

Fig. 16. Cassegrainian geometry and equivalent parabola.

$\text{TAN}(\phi_m/2) = D_m/4F_m$

$F_e/F_m = L_s/L_v = \text{TAN}(\phi_m/2)\big/\text{TAN}(\gamma_o/2) = M$ (magnification factor)

$$TE_{11} \begin{cases} E_x = j \dfrac{\omega\mu k_{11}}{2} J_2(k_{11}r) \sin 2\varphi & (2) \\ E_y = j \dfrac{\omega\mu k_{11}}{2} [J_o(k_{11}r) - J_2(k_{11}r) \cos 2\varphi] & (3) \end{cases}$$

$$k_{11}a = 1.841$$

$$TM_{01} \begin{cases} E_x = -kk_{01} J'_o(k_{01}r) \cos\varphi & (4) \\ E_y = -kk_{01} J'_o(k_{01}r) \sin\varphi & (5) \end{cases}$$

$$k_{01}a = 2.405 \quad .$$

The far-field components produced by these aperture fields are given by the expressions

$$TE_{11} \begin{cases} E_{xE} = E_{XH} = 0 \\ E_{yE} = -e^{-jkR} \dfrac{ka\omega\mu}{2R} J_1(k_{11}a)(1 + \cos\gamma) \dfrac{J_1(ka \sin\gamma)}{ka \sin\gamma} & (6) \\ E_{yH} = -e^{-jkR} \dfrac{ka\omega\mu}{2R} J_1(k_{11}a)(1 + \cos\gamma) \dfrac{J'_1(ka \sin\gamma)}{1 - (ka \sin\gamma/k_{11}a)^2} & (7) \end{cases}$$

$$TM_{01} \begin{cases} E_{xE} = E_{yH} = 0 \\ E_{xH} = E_{yE} = j e^{-jkR} \left(\dfrac{-kk_{01}2\pi a^2}{2\lambda R}\right) J_1(k_{01}a)(1 + \cos\gamma) \\ \qquad \cdot \dfrac{J_o(ka \sin\gamma)}{ka \sin\gamma [1 - (k_{01}a/ka \sin\gamma)^2]} \quad . & (8) \end{cases}$$

The maximum feed-horn gain for both modes is given by

$$TE_{11} \qquad G_f = 0.837 (ka)^2 \qquad (9)$$

$$TM_{01} \qquad G_f = 0.256 (ka)^2 \quad . \qquad (10)$$

Now we have the feed-horn pattern and gain expressions, and by using Eq. (1) we can compute the antenna efficiency. If we do this for the TE_{11} mode, which is our main interest, we get for the antenna efficiency,

$$\eta = \frac{1}{4} \left[\cot^2 \frac{\gamma_o}{2}\right] 0.837 (ka)^2 \left| \int_o^{\gamma_o} [F_1(\gamma) \cos\gamma + F_2(\gamma)] \sin\gamma \, d\gamma \right|^2 \qquad (11)$$

where

$$F_1(\gamma) = \frac{J_1(ka \sin\gamma)}{ka \sin\gamma} \quad , \quad F_2(\gamma) = \frac{J'_1(ka \sin\gamma)}{1 - (ka \sin\gamma/k_{11}a)^2}$$

are essentially the E- and H-plane TE_{11} mode patterns.

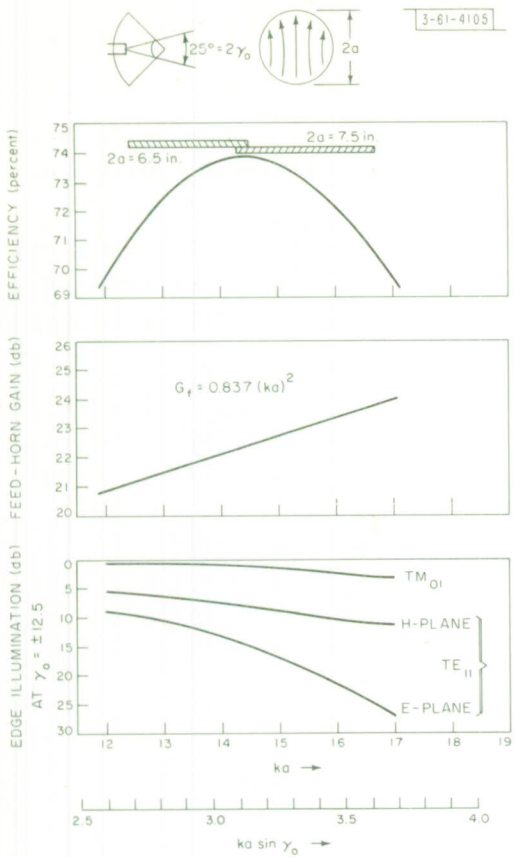

Fig. 17. TE_{11}-mode feed-horn antenna efficiency.

This expression has been machine-computed and the result is given in Fig. 17. Although computed for $\gamma_o = 12.5°$, the results are valid for any value of ka $\sin\gamma_o$, since no small-angle approximations have been used. The maximum efficiency of 73.8 percent is reached for a value of ka $\sin\gamma_o = 3.14$, or about -11-db average edge illumination of the subreflector. These results are consistent with the calculations carried out by Dion[8] on other simple feed-horn geometries. Figure 17 shows that to achieve maximum efficiency for the 7.2- to 8.4-GHz band, we must use $13.5 \leqslant ka \leqslant 15.8$ or $7.05 \text{ inches} \leqslant 2a \leqslant 6.05$ inches. In order to cover the regions indicated, it was decided to build and test two aperture sizes, 7.5 and 6.5 inches in diameter. The conical-horn-reflector aperture diameter was fixed at 7.5 inches before any experimental data were available; however, since there are 28 inches of straight waveguide from the feed-horn aperture to the conical-horn reflector aperture, it was thought that any small changes in diameter could be accommodated by a long linear taper. This has since turned out to be so.

A calculation of the antenna efficiency for the TM_{01} mode feed-horn excitation is carried out in Appendix B and we have the result

$$\eta = \frac{(1+\cos\gamma_o)^2}{u_o^2}\left|\int_o^{\gamma_o} \frac{J_1(S)\,J_o(u)}{1-(2.405/u)^2}\,du\right|^2 \qquad (12)$$

where $S = [(\pi D/\lambda)\sin\theta_o]\cot(\gamma_o/2)\tan(\gamma/2)$, $u = ka\sin\gamma$. Now for $D = 180$ inches, $\lambda = 1.47$ inches, $\theta_o = 0.35°$, $\gamma_o = 12.5°$, $ka = 13.9$. Equation (12) has been evaluated and we get the result, $\eta = 0.120$. Now

$$\frac{\eta(TE_{11})}{\eta(TM_{01})} = \frac{0.738}{0.120} = 6.15 \doteq 7.89\,\text{db} \quad .$$

This relation says that the ratio of the maximum gain of the TE_{11} to the maximum gain of the TM_{01} mode feed-horn patterns is 7.89 db. The differences between the measured value and that given above are discussed in Sec. IV.

Since we have computed the feed-horn pattern expressions [Eqs. (6) and (8)], we can now calculate the expected secondary antenna patterns. The following expressions are derived in Appendix A and we give only the final results here. The relative values of the X- and Y-components of the field radiated from the full antenna are given by the following equations:

$$TE_{11} \quad \begin{cases} E_{yE}(\Theta) = A_1 \int_0^{\gamma_o} \left[F_1(\gamma) \cos\gamma\, J_1'(P) + F_2(\gamma)\, \dfrac{J_1(P)}{P} \right] \sin\gamma\, d\gamma & (13) \\ E_{yH}(\Theta) = A_2 \int_0^{\gamma_o} \left[F_1(\gamma) \cos\gamma\, \dfrac{J_1(P)}{P} + F_2(\gamma)\, J_1'(P) \right] \sin\gamma\, d\gamma & (14) \\ E_{xH}(\Theta) = E_{xE}(\Theta) = 0 \end{cases}$$

$$P = \left(\frac{\pi D}{\lambda} \sin\Theta\right) \cot\frac{\gamma_o}{2} \tan\frac{\gamma}{2} \quad , \qquad k_{11}a = 1.841$$

$F_1(\gamma)$ and $F_2(\gamma)$ are given in Eq. (11) .

$$TM_{01} \quad E(\Theta) = A_3 \int_0^{\gamma_o} J_1(P)\, \frac{J_o(ka \sin\gamma)}{1 - (k_{01}a/ka \sin\gamma)^2} \cos\gamma\, d\gamma \qquad (15)$$

$$k_{01}a = 2.405 \quad .$$

These expressions have been machine-computed for some particular values of the constants and the results are given in Fig. 18. The side-lobe structure shown is not considered realistic, since no account of blockage, spillover, or diffraction effects is included in the equations.

D. Feed-Horn Patterns and Gain Measurements

Antenna patterns and gain measurements were taken on both the 6.5- and 7.5-inch aperture feed horns. The patterns were reduced to numerical data and the antenna efficiency was machine-computed using Eq. (1). The results for the 6.5-inch aperture are given in Fig. 19. The measured feed-horn gain is about 0.5 db below the TE_{11} mode theoretical gain, instead of less than 0.15 db as expected.*

This gain loss, of course, makes the antenna efficiency lower by the same amount. The 7.5-inch aperture feed-horn data were very similar except that this horn seems to be slightly poorer in performance at the higher end of the frequency band, probably because of the increased taper at the subreflector edge.

Some of the measured feed-horn patterns are shown in Figs. 20(a-h) and compare closely with the theoretical patterns previously given. The polarization is indicated by a sketch of the horn on each pattern.

*It is interesting to note that Hines, et al.,[1] also report a measured gain value for their conical-horn reflector of 0.515 ± 0.2 db below the corresponding theoretical TE_{11} mode gain.

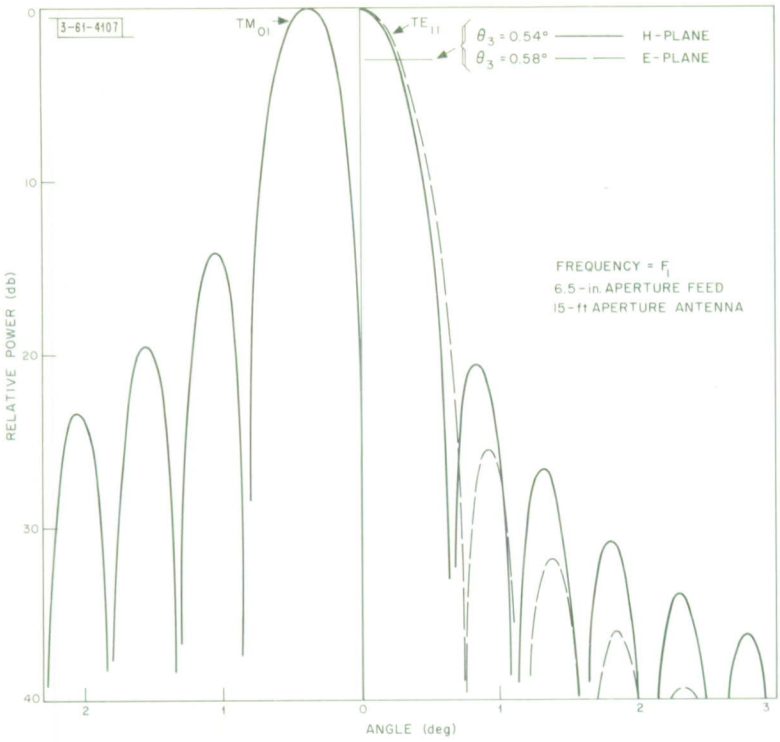

Fig. 18. Secondary antenna patterns (TE_{11} and TM_{01} feed horns).

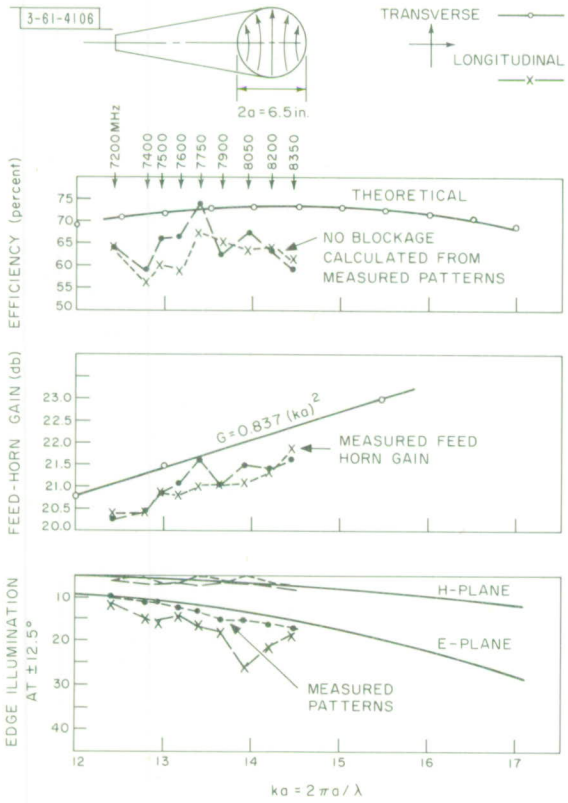

Fig. 19. Measured feed-horn data and computed antenna efficiency.

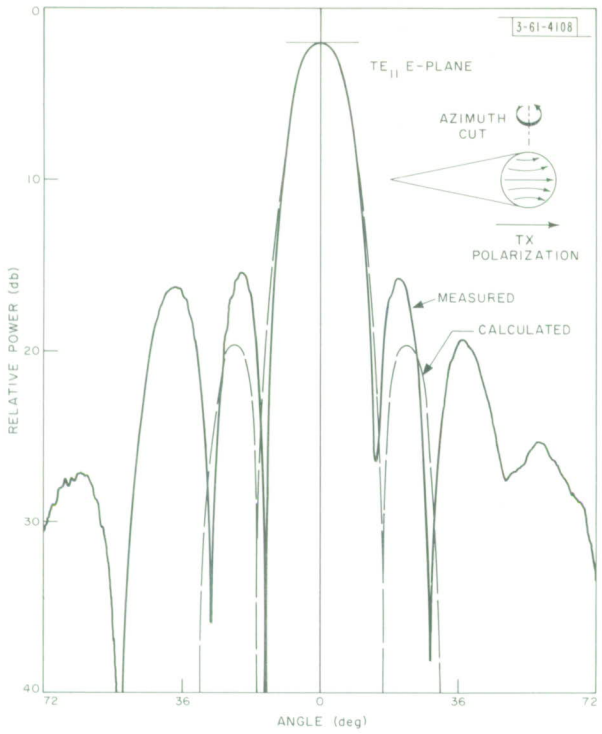

(a)

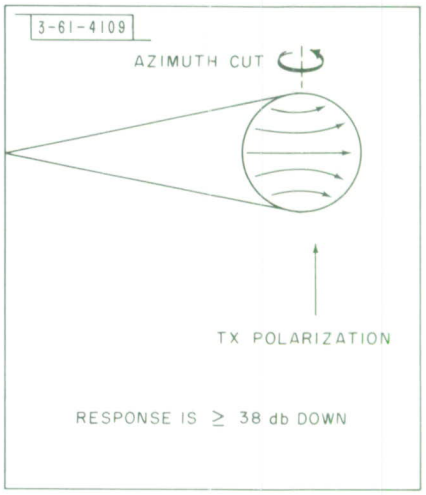

(b)

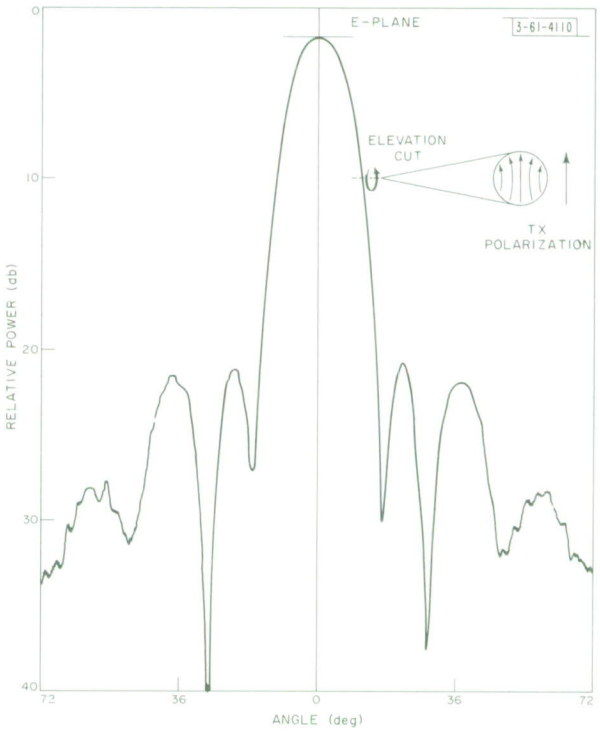

(c)

Fig. 20(a-h). Conical-horn-reflector feed patterns (at F_1 for 6.5-inch aperture).

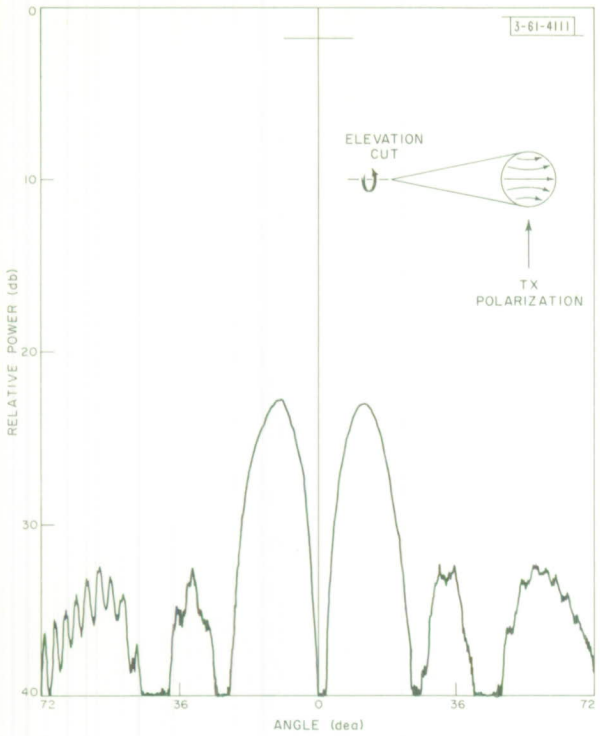

(d)

(e)

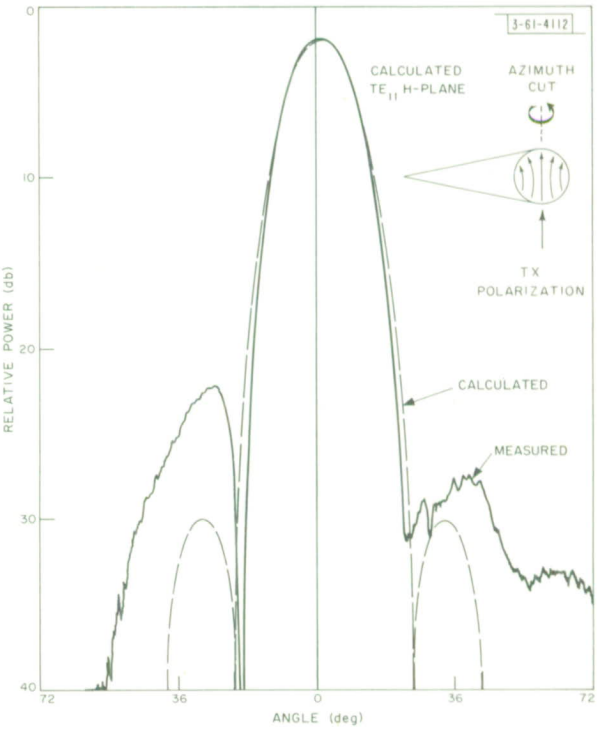

Fig. 20. Continued.

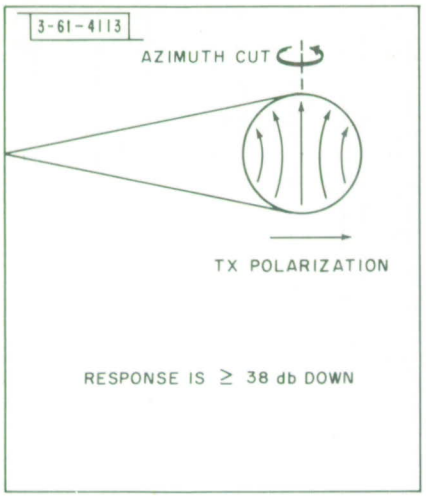

(f)

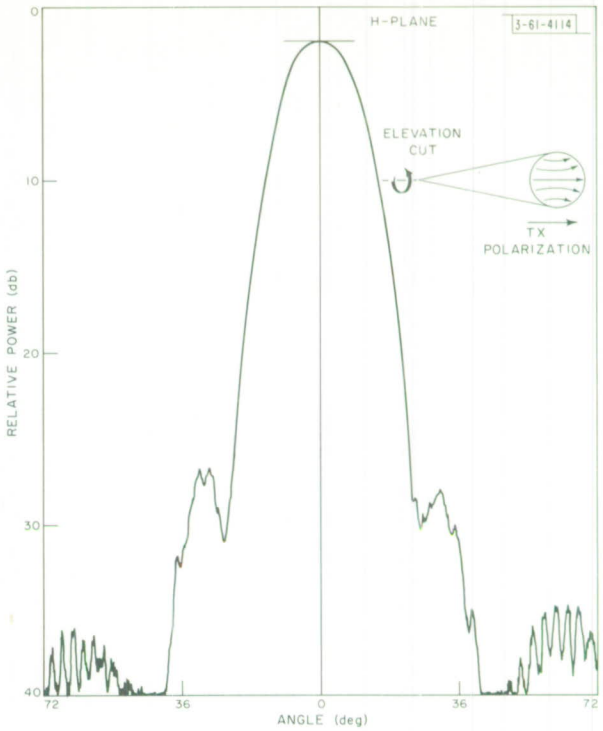

(g)

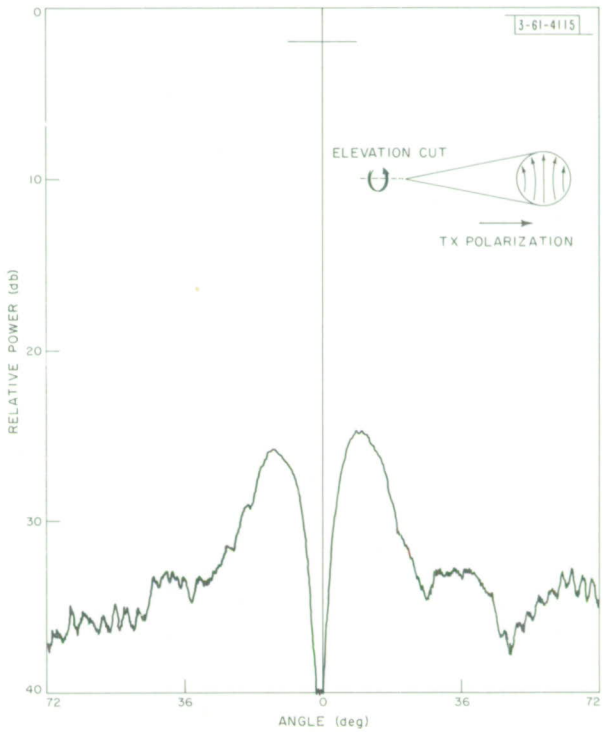

(h)

Fig. 20. Continued.

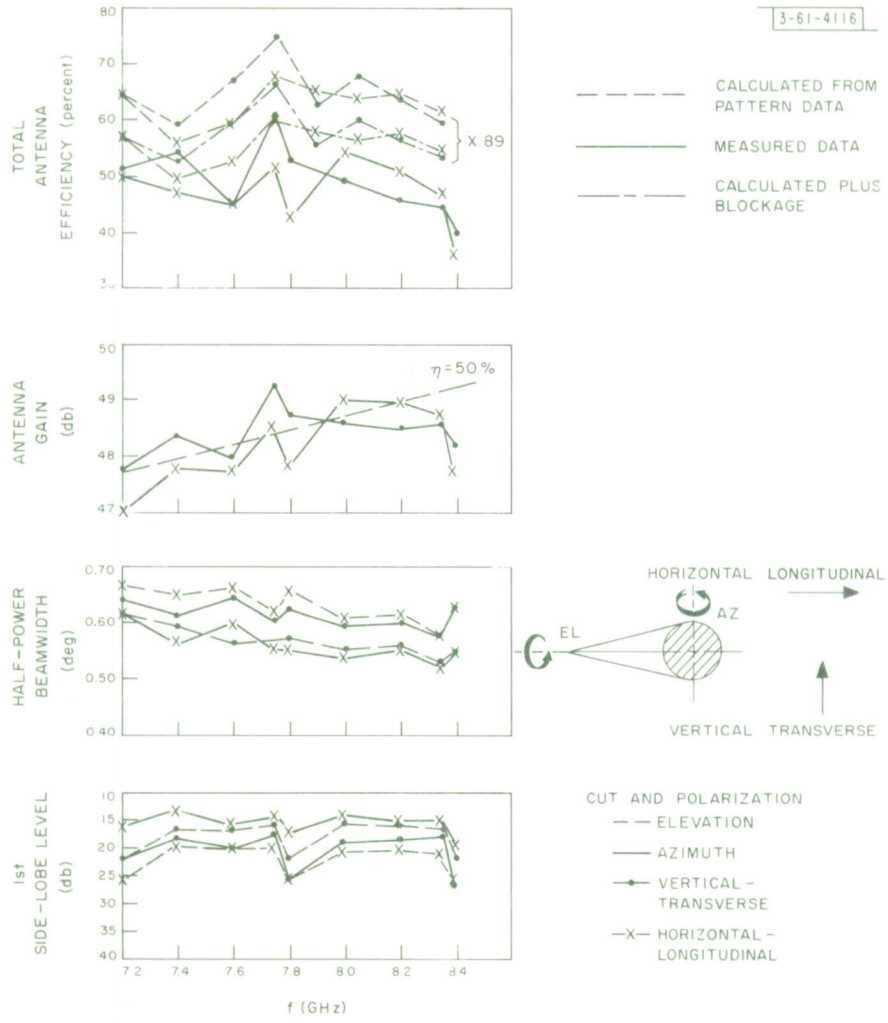

Fig. 21. Final LET antenna data (6.5-inch feed aperture).

E. Measured Secondary Patterns and Antenna Gain

The conical-horn-reflector feed was mounted in the antenna and the antenna system was focused by moving the subreflector along the focal axis. This was done for both the 6.5- and 7.5-inch apertures, F_1 and F_2, and longitudinal and transverse linear polarization. The data taken were the antenna gain and elevation and azimuth plane patterns. The cone axis was always positioned in the horizontal plane. The best subreflector position, based on the criterion of maximum gain and minimum beamwidth, was selected for each aperture. Incidentally, it was found, while focusing, that by sacrificing 0.5 to 0.75 db of gain, side-lobe levels of about −20 db could be achieved. Next a full set of data over the 7.2- to 8.4-GHz band was taken at each subreflector setting for the two apertures. On the basis of these tests, the 6.5-inch aperture was chosen as the better of the two; however, the difference between the two apertures was slight. The final focused position of the subreflector was only 0.042 inch toward the antenna surface from the geometric focus. A summary of the final data is shown in Fig. 21. Both longitudinal and transverse polarization data are shown for the elevation and azimuth patterns. The side-lobe level, beamwidths, gain, and efficiency are also shown over the frequency band.

Some typical antenna patterns are shown in Figs. 22(a-m). These patterns are for linear polarization and the polarization condition is given on each pattern. The feed exciter was replaced by a linear taper for this set of data. Since the test-field cross-polarized component was only about −30 db, the "true" cross-polarized antenna patterns must be much lower than that shown. Complete circularly polarized pattern data were taken using the final feed components, and some of these patterns are shown in Figs. 23(a-f). The cross-polarized patterns depend greatly on the orientation of the rotary joint assembly relative to the fixed feed horn. The "beating" of the different transmitting and receiving, opposite hand, polarization ellipses causes very large variations in received signal, depending, of course, on the axial ratios involved. The "true" cross-polarized antenna response is not known, except that it lies between that shown on the patterns and a null response. More pertinent, however, is the isolation achieved during transmission from the TX-Σ to the REC-Σ ports, and this has been measured to be about −20 db, which is considered satisfactory.

The peak value of the Δ-port patterns [Figs. 23(e-f)] is seen to be about −12.5 db down from the circularly polarized REC-Σ pattern peak. The expected value is 7.89 + 3.0 = 10.89 db. The reason for the difference between the measured and computed values is discussed at length in Sec. IV.

Because of time limitations, the circularly polarized antenna gain data were taken only at F_1 and F_2 and the results referenced to the input terminals of the feed are summarized below.

Frequency (MHz)	Transmitting Polarization	Antenna Gain (db)	Antenna Efficiency (percent)
F_1	RHC	48.51	51.3
F_1	LHC	48.92	56.3
F_2	RHC	48.98	49.3
F_2	LHC	48.80	47.4

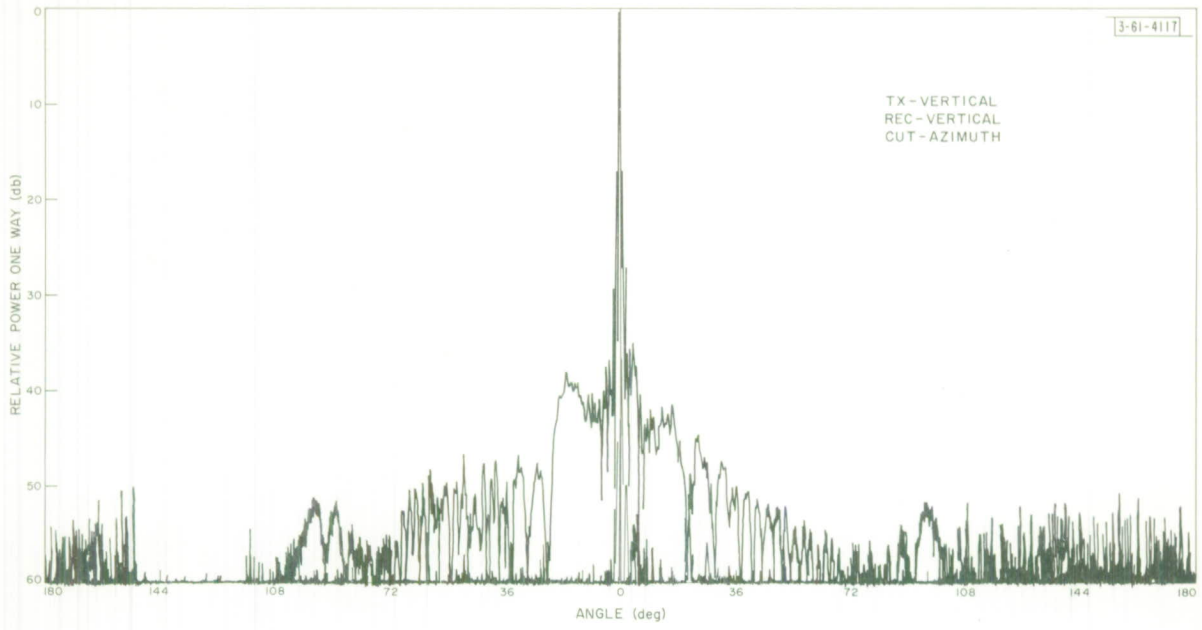

(a)

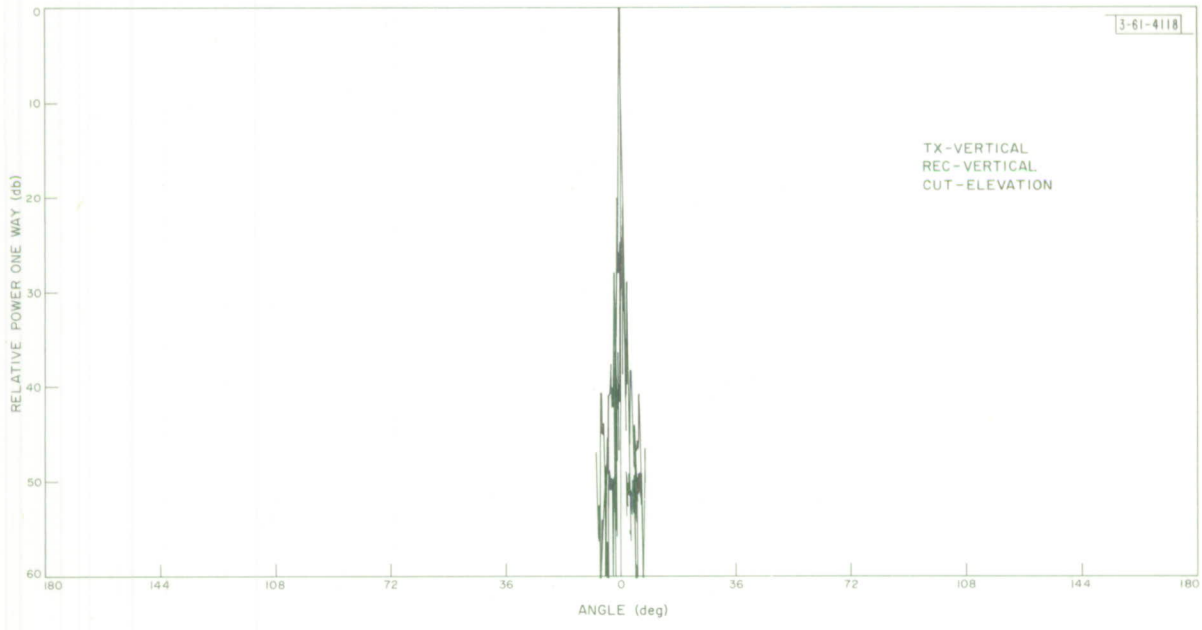

(b)

Fig. 22(a-m). Antenna patterns (linearly polarized at F_1).

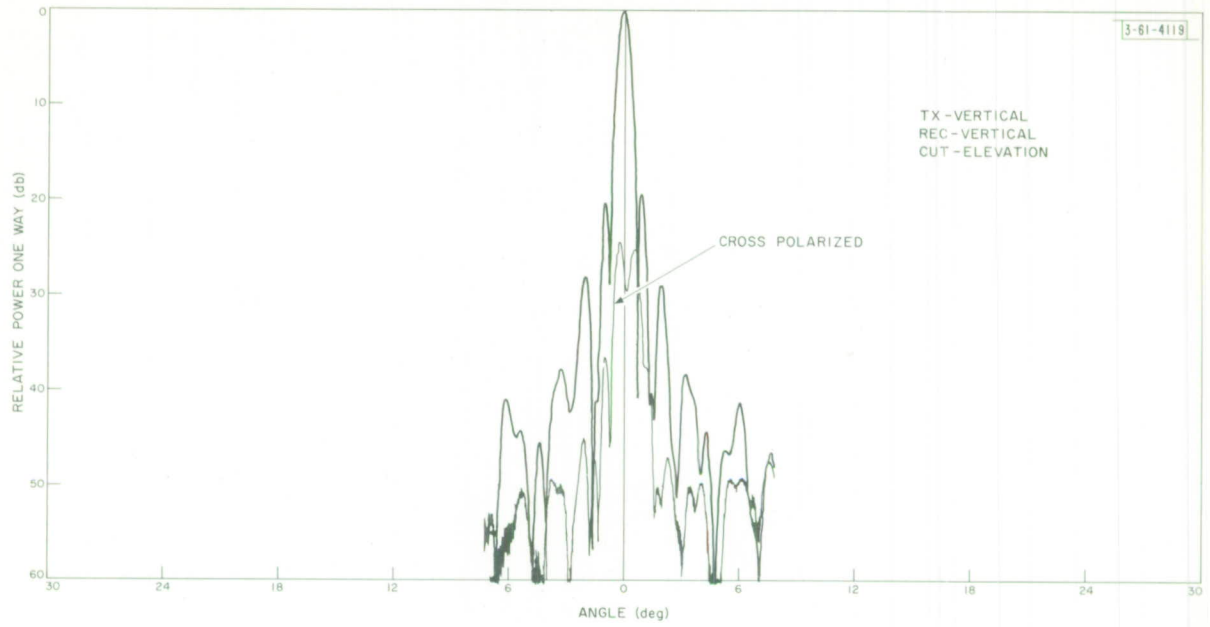

(c)

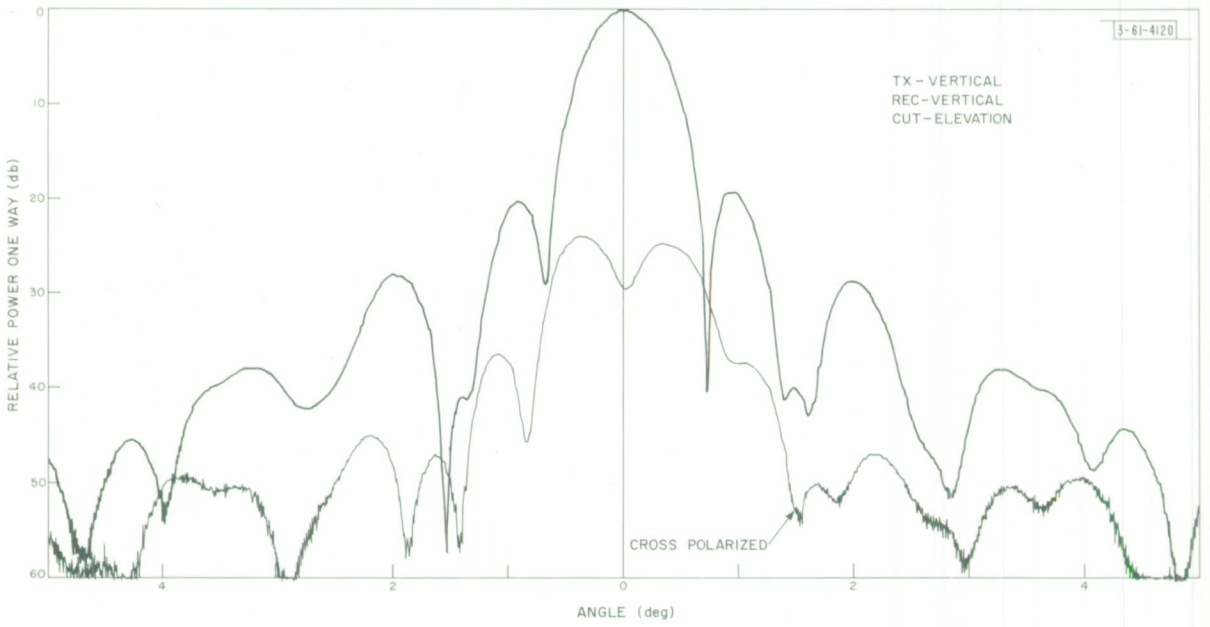

(d)

Fig. 22. Continued.

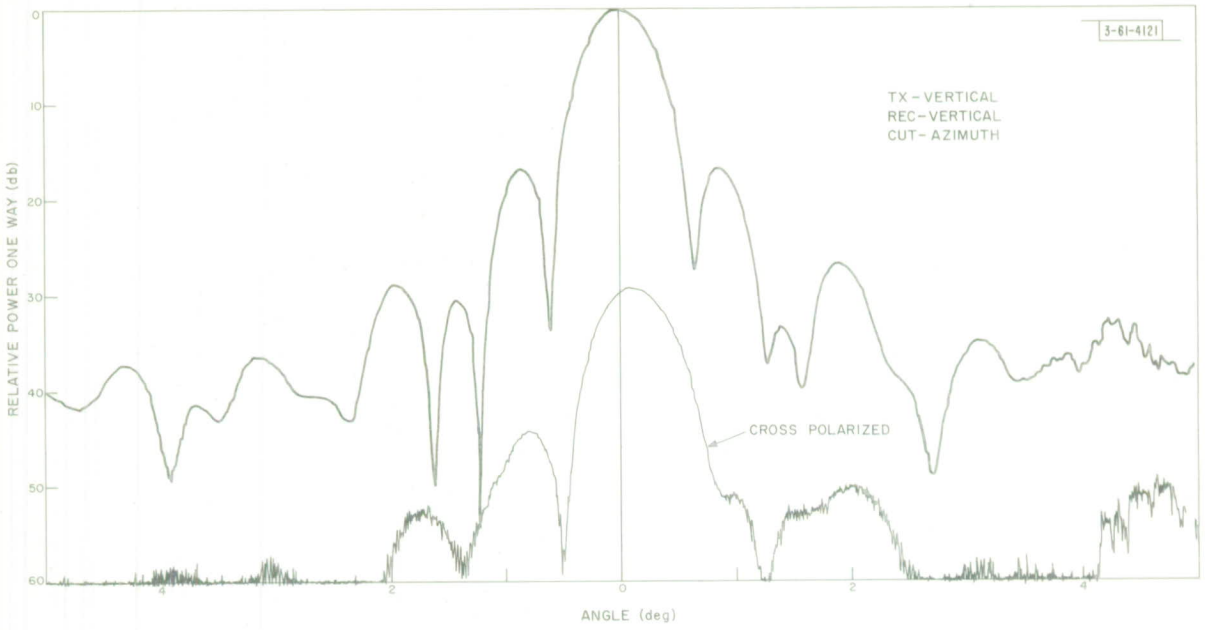

(e)

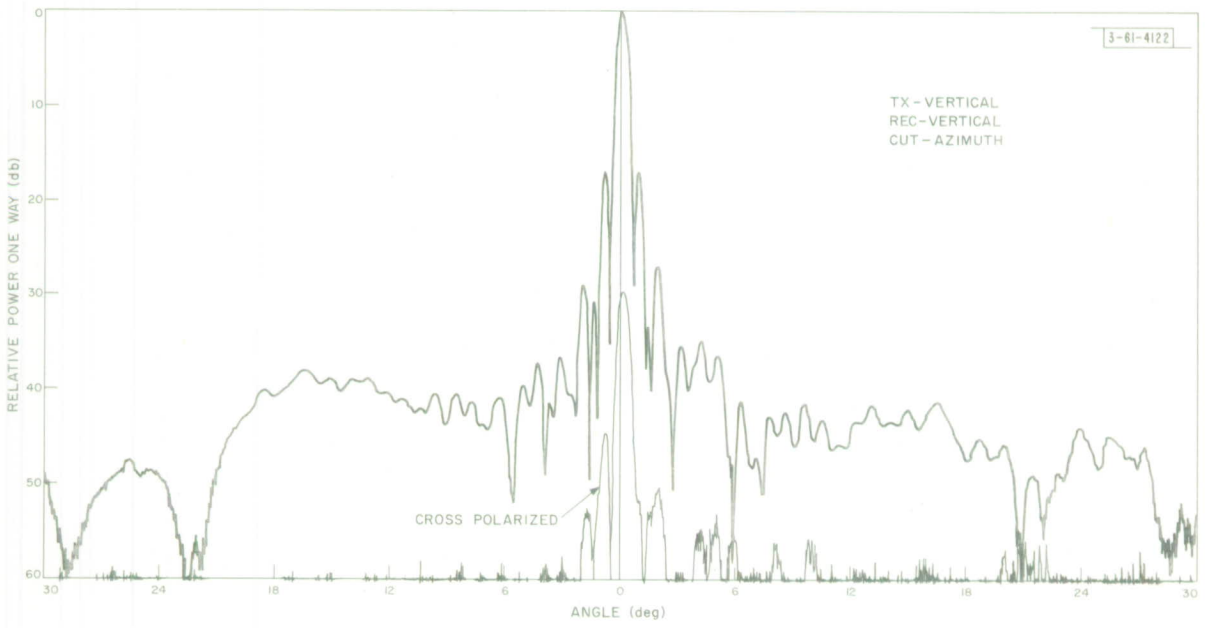

(f)

Fig. 22. Continued.

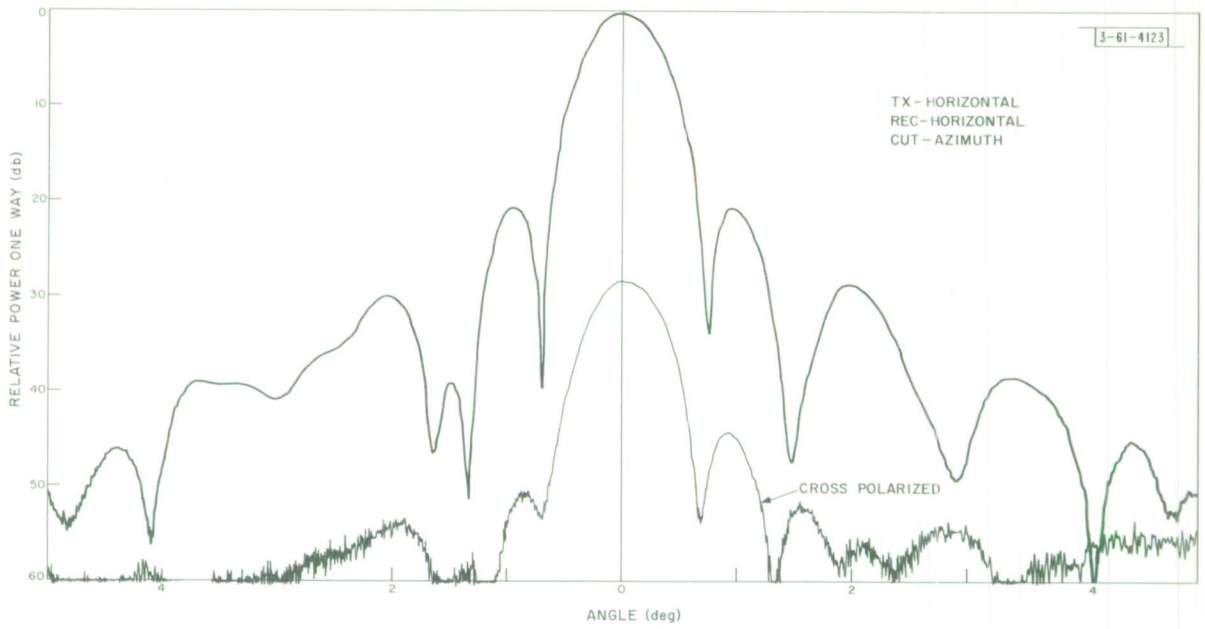

(g)

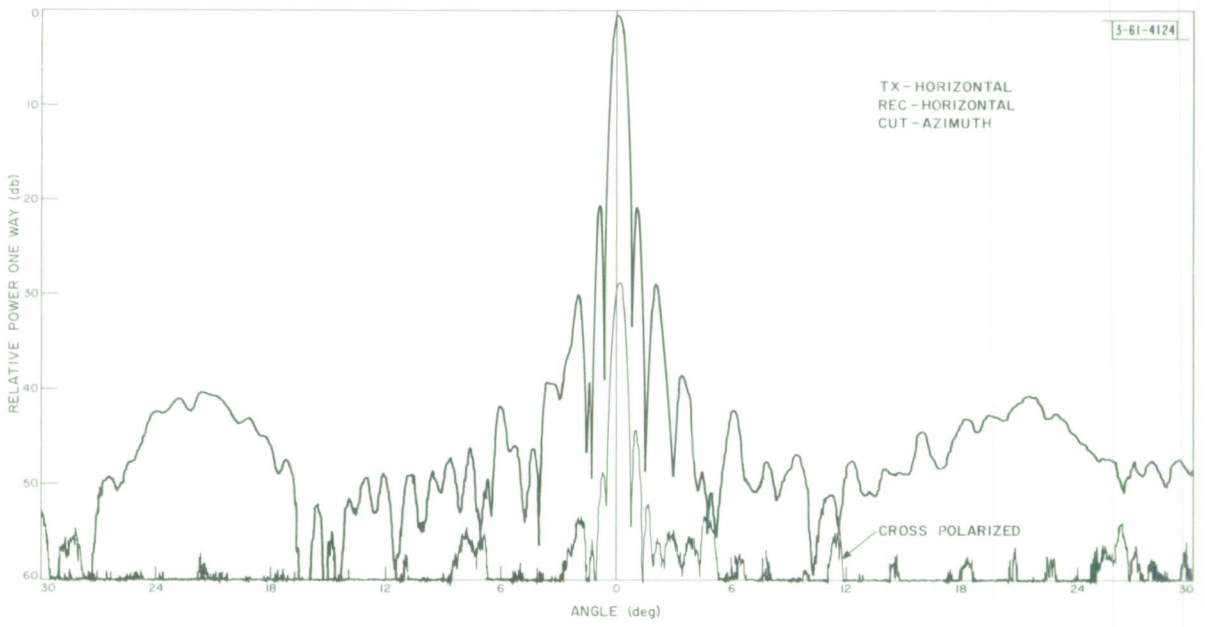

(h)

Fig. 22. Continued.

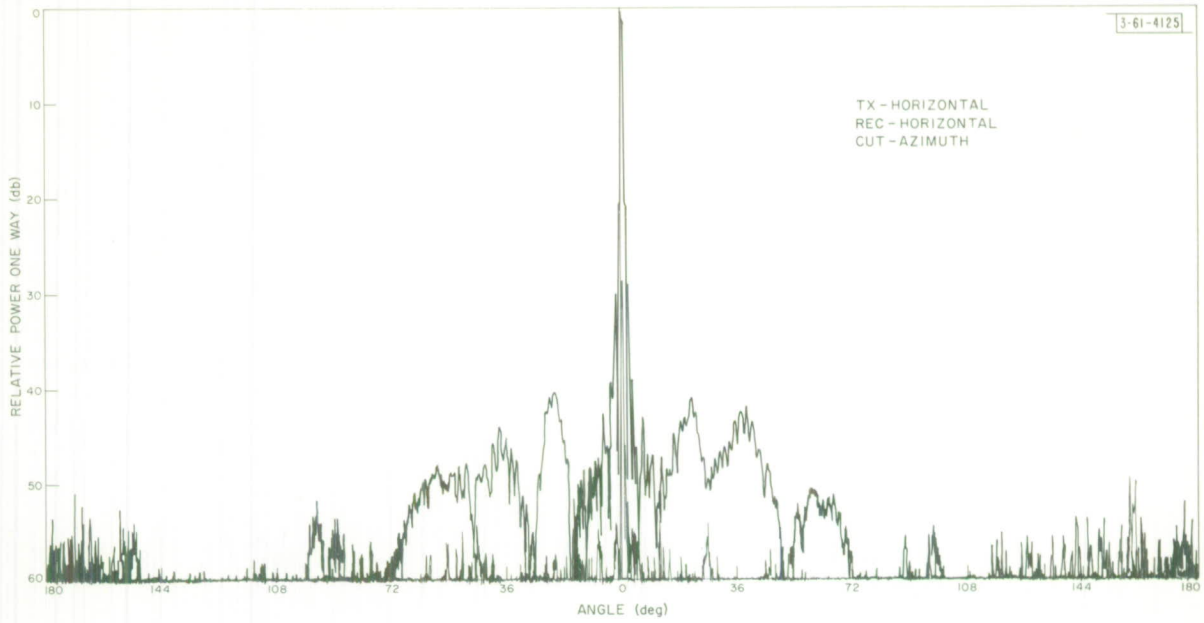

(i)

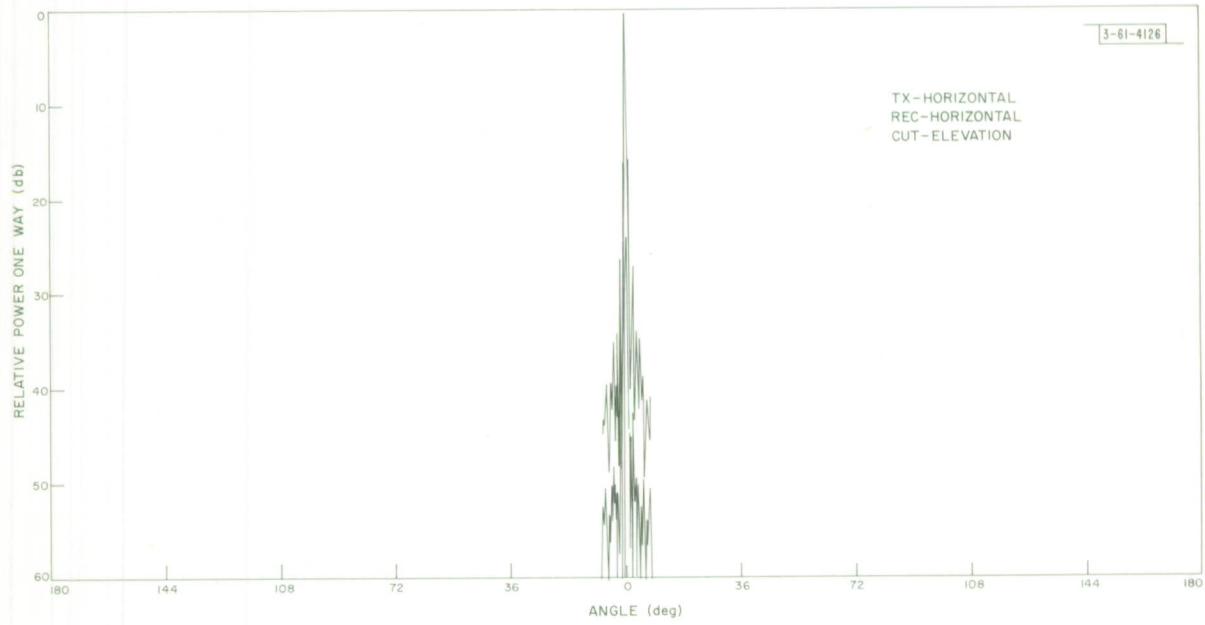

(j)

Fig. 22. Continued.

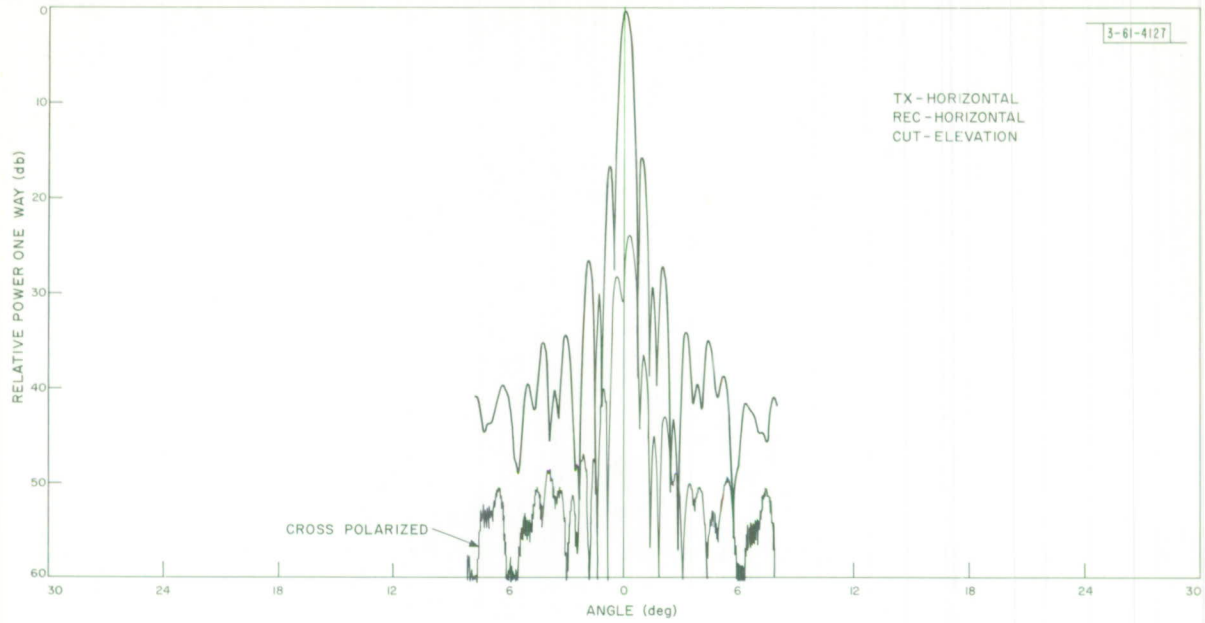

(k)

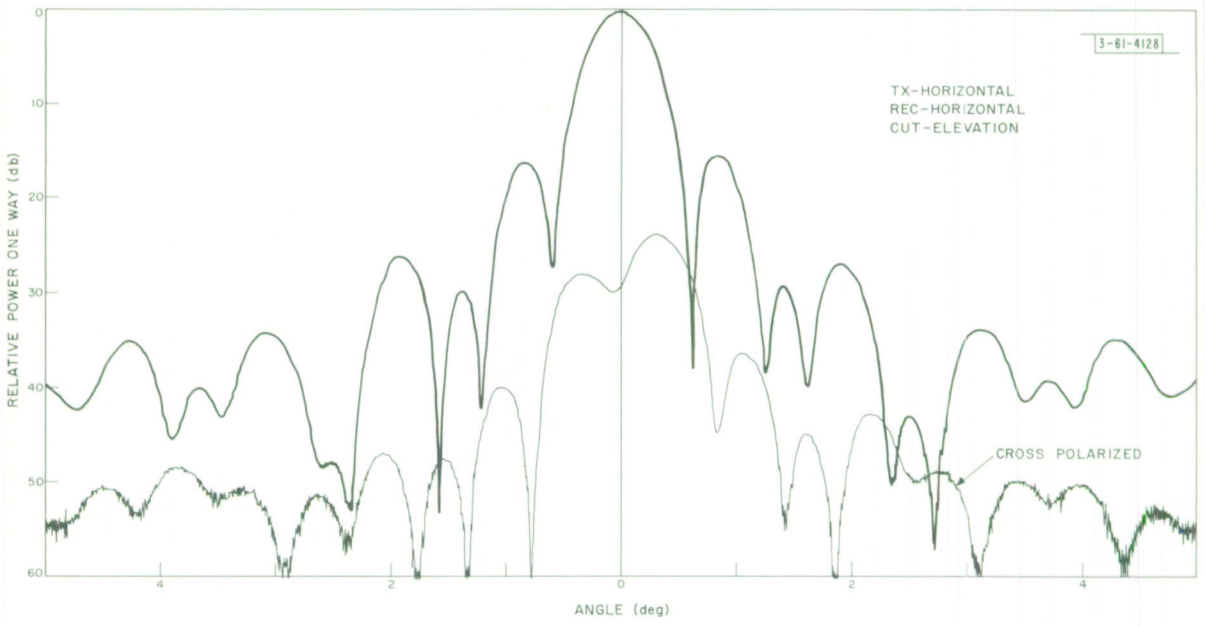

(l)

Fig. 22. Continued.

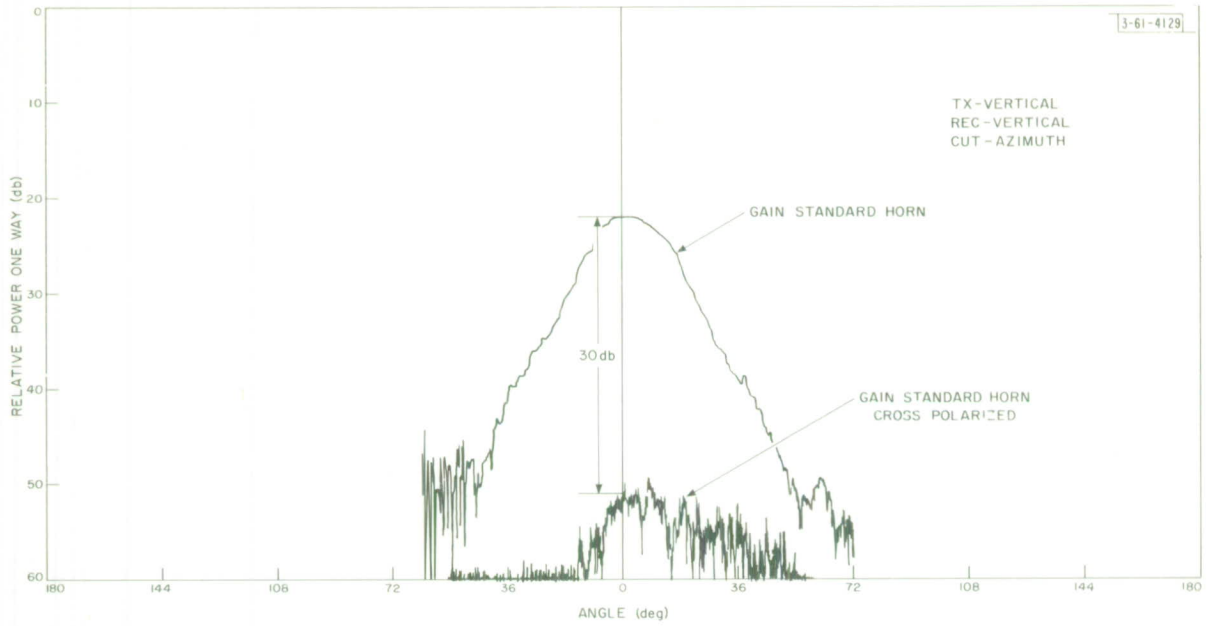

(m)

Fig. 22. Continued.

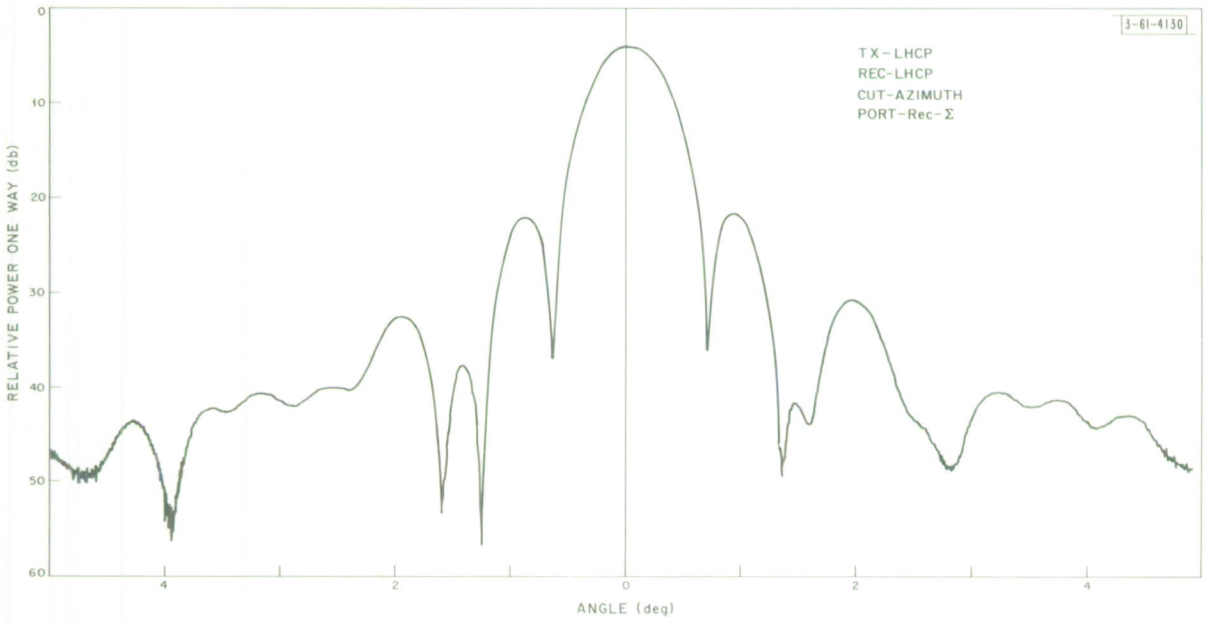

(a)

Fig. 23(a-f). Antenna patterns (circularly polarized at F_1).

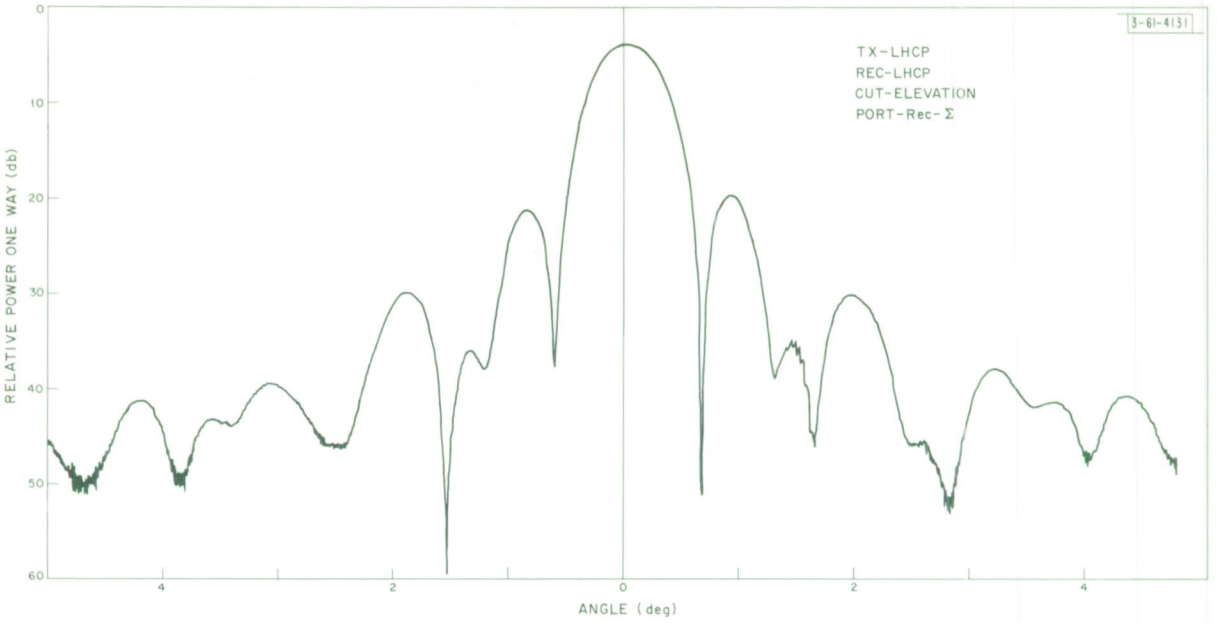

(b)

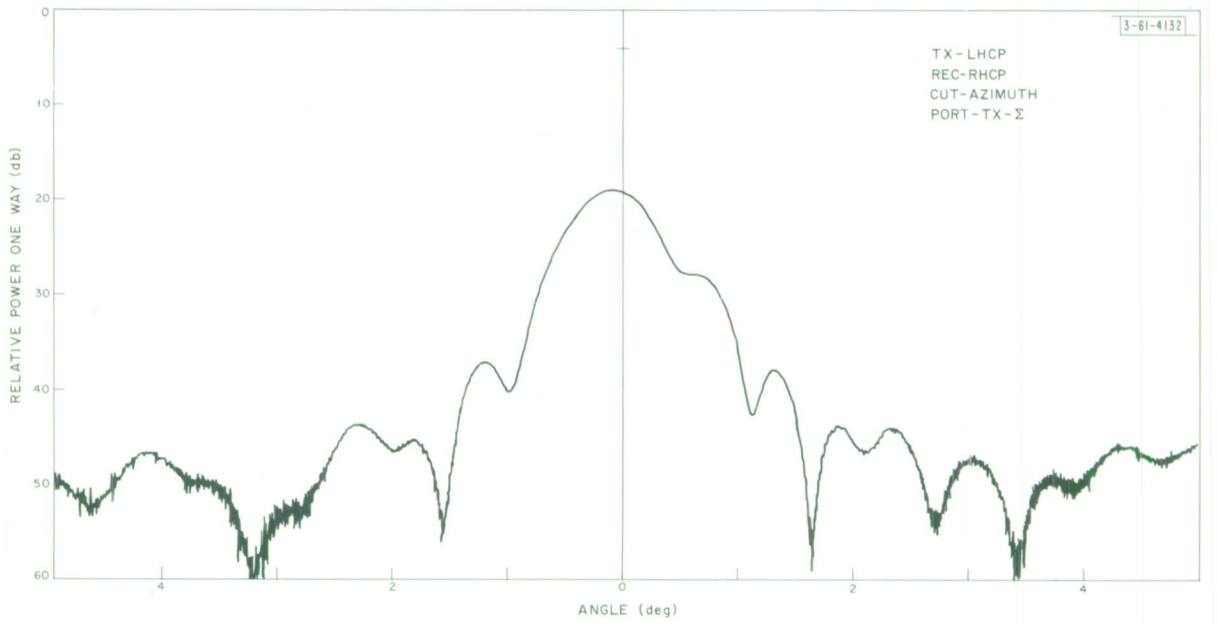

(c)

Fig. 23. Continued.

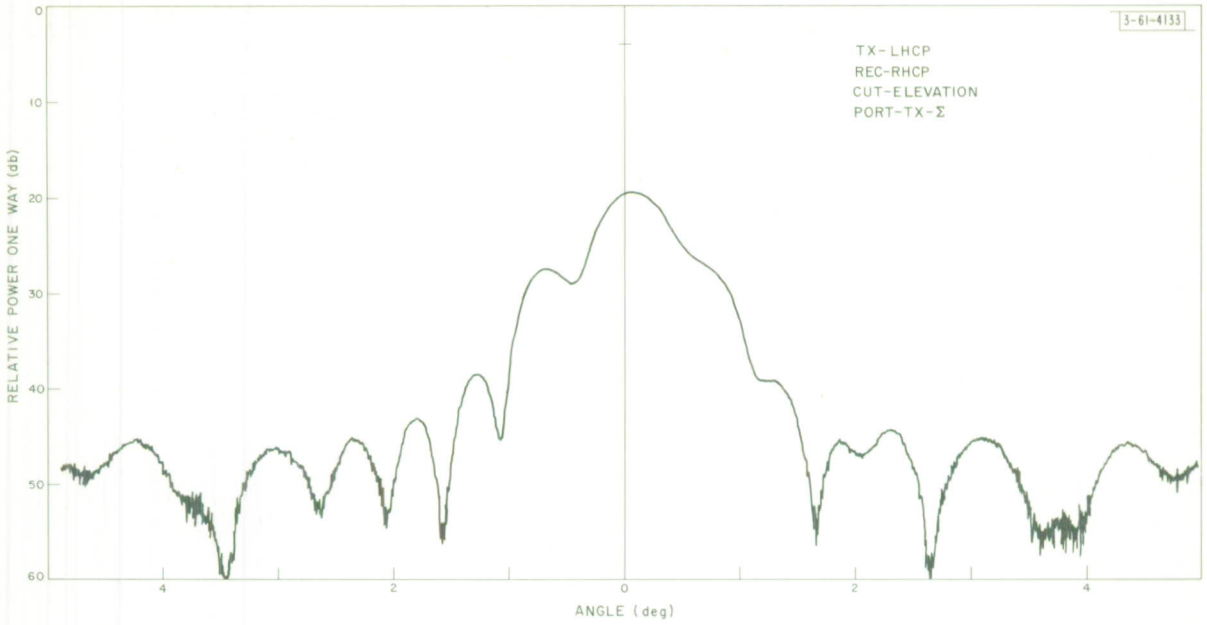

(d)

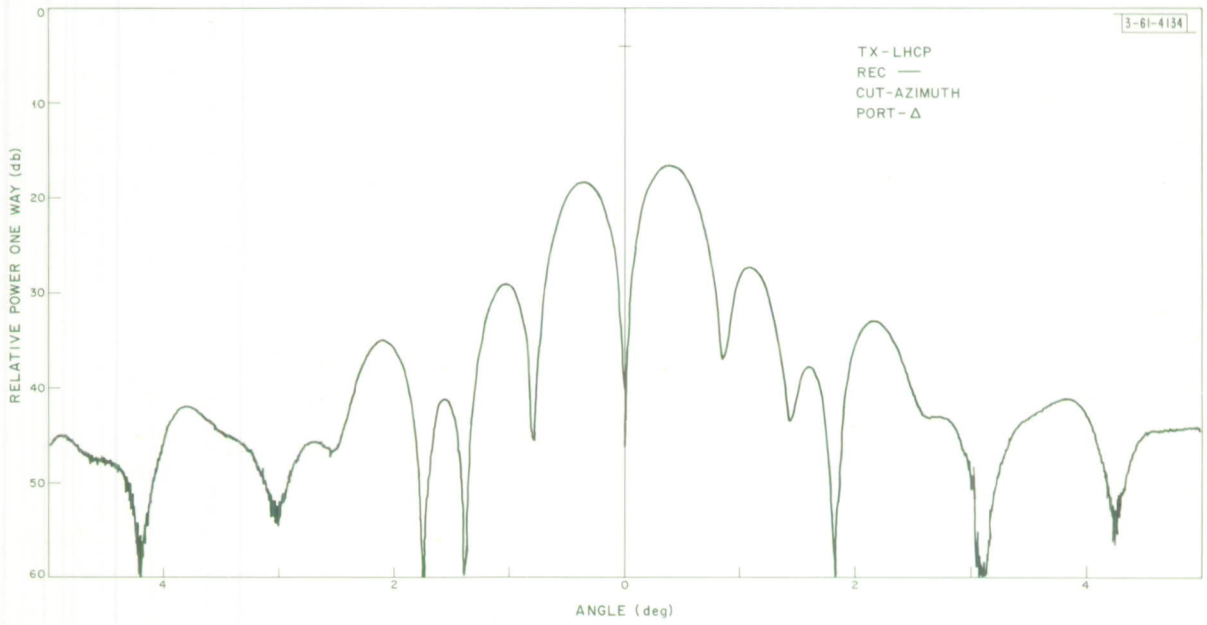

(e)

Fig. 23. Continued.

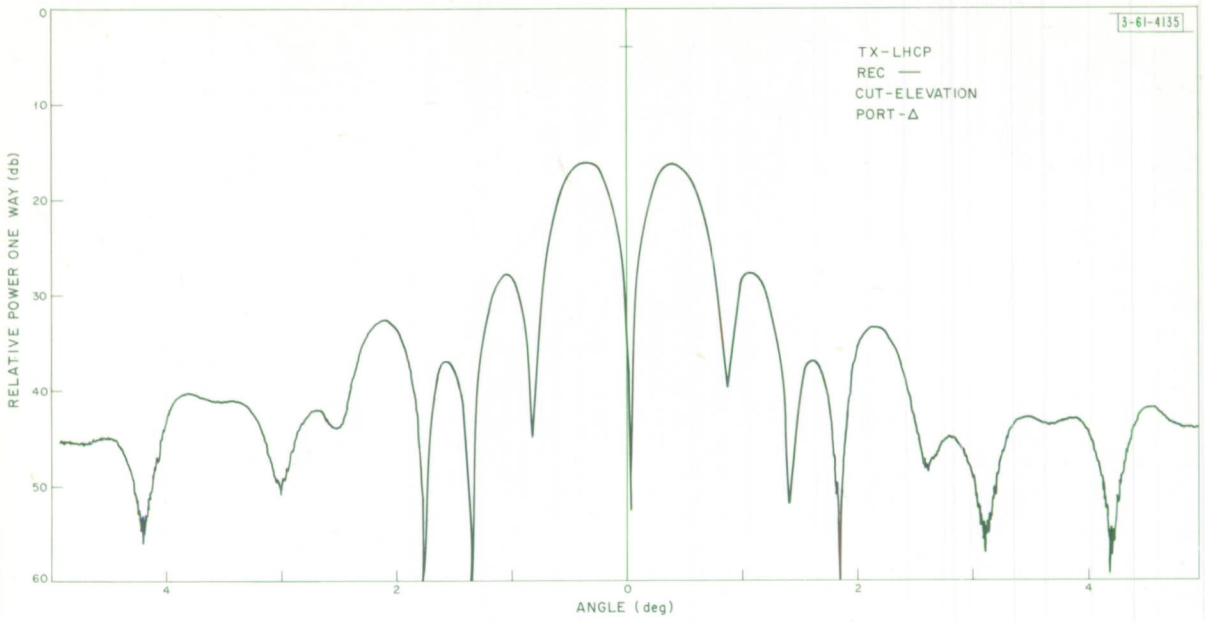

(f)

Fig. 23. Continued.

F. Subreflector and Boom Blockage, Phase Error Effects, and K-Band Data

The approximate effect on the antenna performance of aperture blockage and surface phase error is well known, and some estimates of the gain loss are calculated in Appendix C. The results are given below.

Effect	Calculated Gain Loss (db)
Subreflector blockage	0.264
Boom blockage	0.226
Phase error (0.013 inch rms)	0.014
Total	0.504 db = 0.89 = η_L

We must now multiply our theoretical efficiency by η_L to get the final value, including blockage effects. This is shown in Fig. 21 along with the measured and computed values.

The blockage will also increase the side-lobe levels. For a nominal 20-db side-lobe level, we compute an increase to −15.7 db. This is the approximate side-lobe level that is actually observed.

In order to have an independent measurement of the blockage effects and also feed-horn variations before the LET antenna was available, a 3:1 reduced-scale model of the full-size 15-foot antenna was constructed. This 5-foot paraboloid operates at 24 GHz and is shown in Fig. 24. (The streaks on the surface are caused by the peeling of a very thin Hypalon coating and do not represent the true surface condition, which was quite good.) The blockage of booms

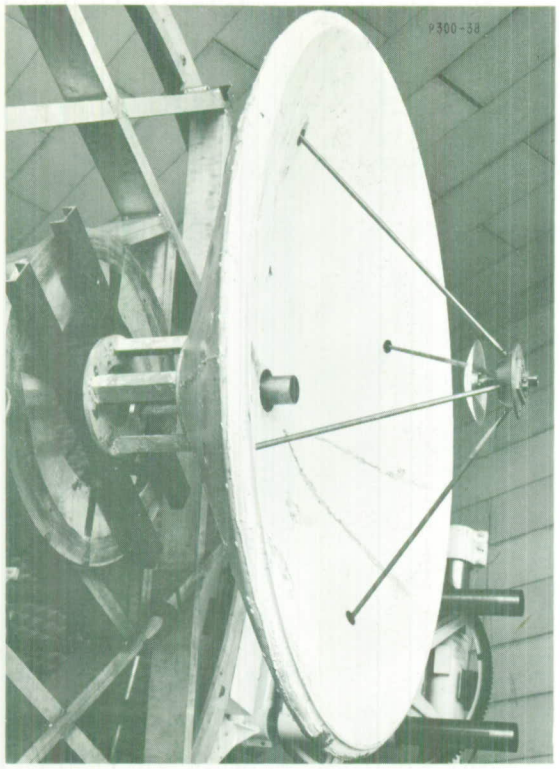

Fig. 24. Scale model of LET antenna (K-band).

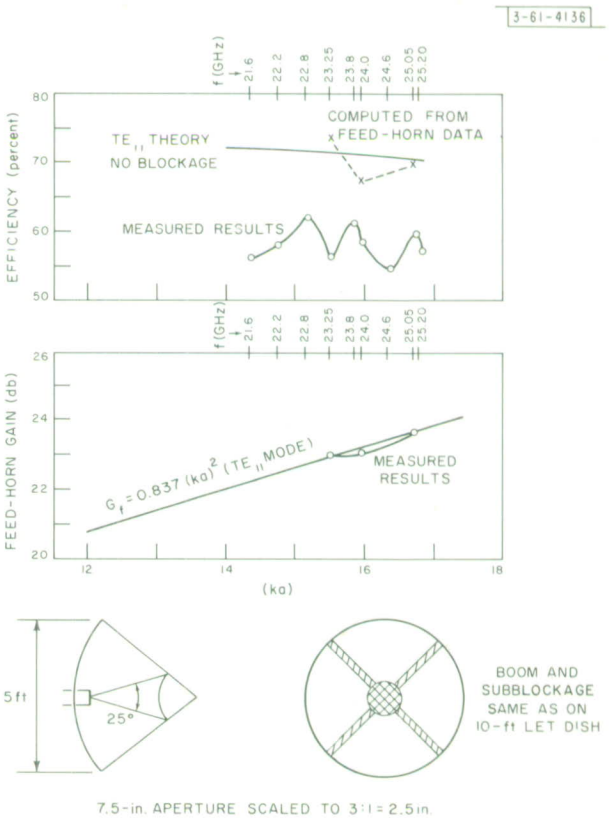

Fig. 25. Data on scale model antenna.

and subreflector was kept identical in the scale model compared with the full-size antenna. The feed horn, however, was an open-ended circular waveguide and not a conical-horn-reflector-fed waveguide. The results of some measurements and calculations are given in Fig. 25. The feed-horn gain is now almost exactly equal to the theoretical value, and the antenna efficiency computed from the measured feed-horn gain and patterns is within a few percent of the theoretical values. The measured antenna efficiency, however, is about 0.85 db below the calculated value. This is about the same difference between theory and measurement found in the full-size antenna. Also, the K-band patterns are similar to the X-band patterns, especially the 16-db side-lobe levels. Subtracting the 0.5-db blockage loss, we find that the unresolved difference between the computed and measured efficiencies of both the X- and K-band antennas is about 0.35 db. It is shown in Sec. IV that this difference is probably explained by scattering and diffraction effects which are not accounted for in our geometric optics approximations.

G. Radome Assembly

The feed is pressurized to about one psi, and to seal the feed system a matched radome is required. Since the pressure is low, one can use either a very thin dielectric sheet ($\approx$10 mil) or a double-wall resonant structure. The double-wall construction was selected because of the possibility of damage to an unprotected thin membrane in an outdoor environment. Teflon sheets of 1/16- and 1/32-inch thickness were investigated experimentally by placing the double sheet on the feed-horn aperture with various spacers. The reflection coefficient vs frequency was displayed on an oscilloscope by using swept frequency techniques, and the lowest average reflection was easily found. The final data are shown in Fig. 26(a). The final radome assembly can be seen in Fig. 2. The input VSWR of the feed is slightly different when mounted in the antenna because of the subreflector reflection. This reflection is small, about equivalent to a VSWR of 1.06:1. Since the reflection is many wavelengths removed from the input of the feed, the phase varies very rapidly with frequency and no optimization over the band is possible. The VSWR of the radome and feed measured in the antenna is given in Fig. 26(b). The maximum temperature rise of the radome is estimated to be about 100° F when transmitting 25-kw CW power. This estimate is based on previous experience with a similar radome system[2] and the physical properties of the Teflon sheet.

H. Antenna Pattern Range

The LET antenna was mounted on an EL-AZ mount [Fig. 3(b)] and placed about 40 feet above the ground to ensure a reflection-free range with a transmitter source located 2000 feet away. Before mounting the antenna, the region to be occupied by the antenna was probed by a small horn mounted on a motor-driven carriage. Automatic height-gain runs were made over a ±8-foot width and up to ±10 feet in height. The maximum variation of the received signal over this entire area was only ±0.2 db, for both horizontal and vertical polarizations. All the antenna data reported here were taken at the Lincoln Laboratory Antenna Test Range which has been described previously.[9] Gain measurements were made by comparison with a standard-gain horn, using a precision waveguide attenuator, and are believed to be accurate to within ±0.25 db.

IV. DISCUSSION OF RESULTS

The antenna gain and efficiency calculations in this report have been based on a simplified geometric optics approximation to the problem. Actually, even for moderate-size hyperboloids

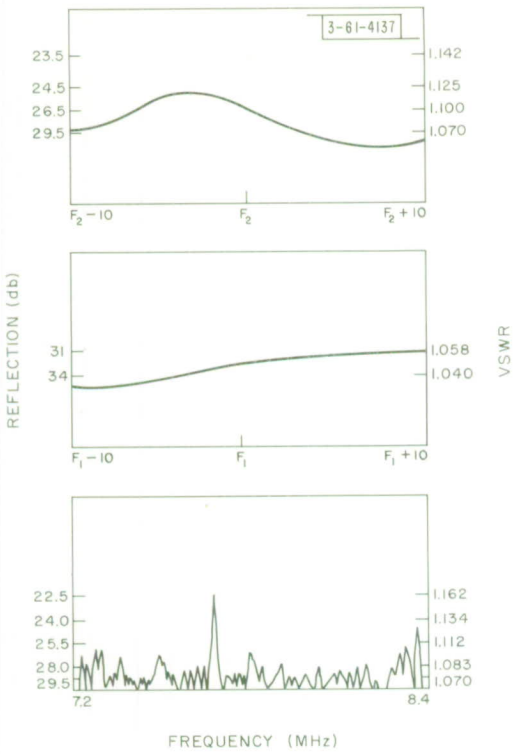

(a) Feed only.

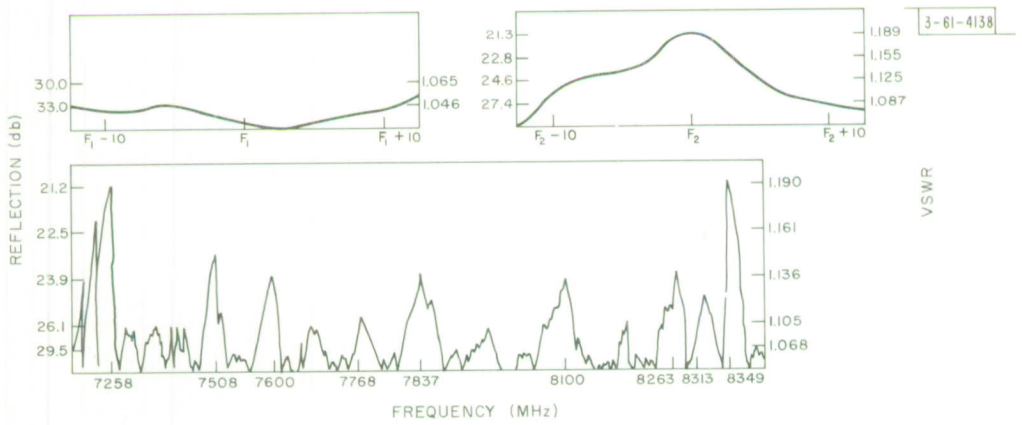

(b) Feed in antenna.

Fig. 26. Radome reflection.

as shown by Rusch,[10] there is a significant amount of scattering from, and diffraction around, the subreflector that is not predicted by the ray-optics approach. This effect produces additional losses not taken into account by Eq. (1). Figure 27 shows the qualitative differences between the diffraction and ray-optics situations. The field from 0° to 77.4° illuminates the paraboloid, the field between 77.4° and 90° is spilled over beyond the paraboloidal edge, and the field between 90° and 180° is called "forward spillover." When the feed-horn pattern is tapered in amplitude, the edge effects are reduced and the spillover losses are less, but are still not negligible.

Equation (1) predicts a theoretical paraboloidal efficiency of 0.738 with the TE_{11} mode feed-horn excitation. The fraction of the feed-horn radiated power available to the paraboloid (η_p) is estimated as 0.85. Then we have

For ray optics: $\eta_{T1} = 0.738 = \eta_{a1} \times \eta_{p1} = \eta_{a1} \times 0.85$

or $\eta_{a1} = 0.869$ (aperture taper efficiency) .

For diffraction: $\eta_{T2} = \eta_{a2} \times \eta_{p2} = \eta_{a1} \times \eta_{p2} = 0.869 \times \eta_{p2}$.

From the data given by Rusch we have $\eta_{p2} \simeq 0.81$ or

$$\eta_{T2} = 0.869 \times 0.81 = 0.704 \quad .$$

The ratio of the efficiencies for the two cases is given by

$$\frac{0.738}{0.704} = 1.05 \equiv 0.212 \text{ db} \quad .$$

The measured difference between the ray-optics theoretical and the experimental results is 0.35 db, which is quite close to the computed ratio of 0.212 db. Other losses, such as feed-horn

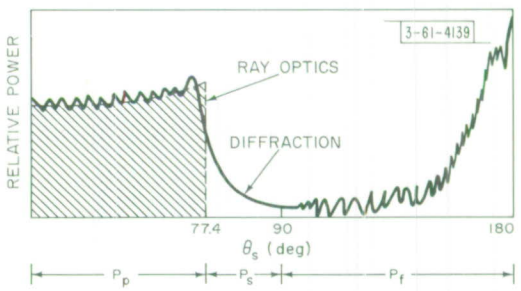

Fig. 27. Ray optics and diffraction comparison.

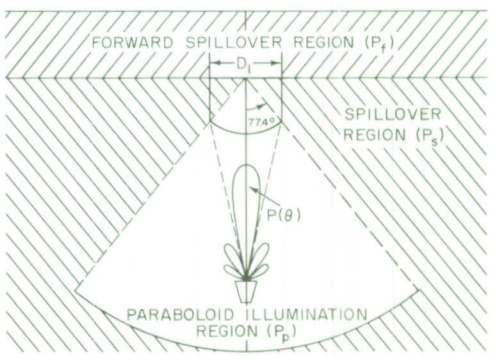

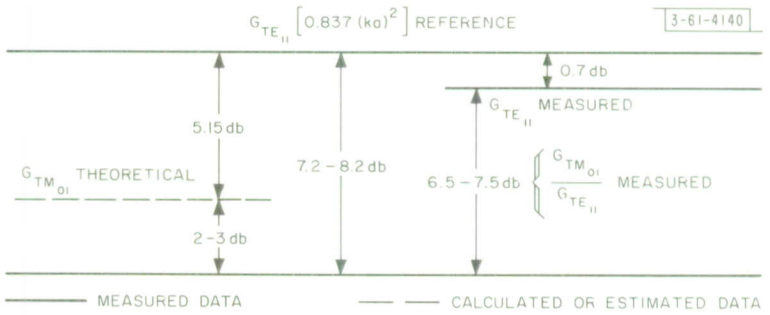

(a) Primary.

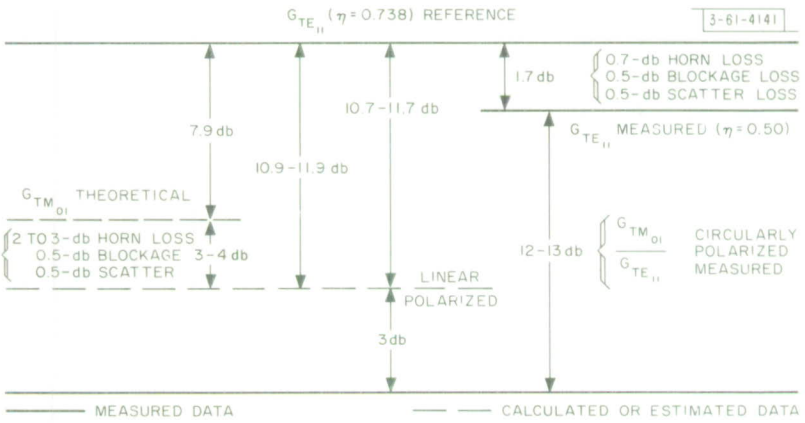

(b) Secondary.

Fig. 28. Gain data analysis (8 GHz).

gain loss, blockage and phase-error loss, are common to both methods and hence do not influence the efficiency ratio. Generally speaking, the diffraction analysis is more exact, and is most useful for determining the total distribution of feed-horn energy. However, it is more convenient to determine the optimum feed-horn configuration by the approach presented here.

To present a clearer picture of the experimental results, the primary feed horn and secondary antenna gain data have been summarized in Figs. 28(a-b). Figure 28(a) shows that the measured TE_{11} excited feed-horn gain is 0.7 db below the theoretical reference gain level (Fig. 19). Also, the measured TM_{01} excited feed-horn gain is 6.5 to 7.5 db below the TE_{11} mode gain. The theoretical difference should be 5.15 db, as computed in Appendix A. The measured data are seen to be 2 to 3 db below this value. Now turning to the secondary gain data [Fig. 28(b)], we see first that the TE_{11} mode excited antenna gain is 1.7 db below the reference value (0.500/0.738). The approximate losses that make up this value are also listed on the figure. Now the measured circularly polarized gain ratio between the TM_{01} and TE_{11} mode cases is 12 to 13 db. The linearly polarized data were not taken but we can assume that the gain is 3 db higher owing to the fact that the TM_{01} mode responds to only one component (radial) of the circularly polarized field. This gives us the value of 10.7 to 11.7 db as the expected gain ratio of the TM_{01} response over the TE_{11} reference. Now the TM_{01} theoretical gain ratio is 7.9 db, as given before (Sec. III-C). By adding the 2- to 3-db measured feed-horn loss and the same blockage and scatter losses assumed for the TE_{11} case, we finally arrive at a gain value of 10.9 to 11.9 db from the reference. This value agrees well with the measured 10.7- to 11.7-db value. This exercise really proves only that the measured data are consistent. The only unexpected value is the 2- to 3-db TM_{01} feed-horn gain loss. Some of this gain loss, as in the TE_{11} mode, is due to the excitation of higher-order modes, by nonperfect mode generation and also by the effect of the amplitude taper across the conical-horn-reflector aperture as mentioned before. However, the total TM_{01} gain loss seems quite large and no satisfactory explanation of the total loss is available at this time.

V. SUMMARY

The requirements, design analysis, and performance data for the LET antenna and feed system have been described. The antenna has Cassegrainian optics and a conical-horn-reflector feed exciter which produces opposite-hand circularly polarized transmitting and receiving beams. The antenna has a measured aperture efficiency of about 50 percent over the 7.2- to 8.4-GHz band. There is also a tracking port which, in conjunction with the receive-sum port, is used as a two-channel tracking system. A relatively simple analysis has been used to determine the optimum feed aperture and the antenna efficiency from both experimental and theoretical data.

APPENDIX A
PATTERN CALCULATIONS

The radiation fields of open-ended circular waveguide operated in the TE_{11} mode are given in Silver[11] and repeated below:

$$\begin{cases} E(\Theta) = -\dfrac{ka\omega\mu}{2R}\, e^{-jkR}\, J_1(k_{11}a)\,(1+\cos\Theta)\,\dfrac{J_1(ka\sin\Theta)}{ka\sin\Theta}\,\sin\varphi & \text{(A-1)} \\ E(\varphi) = -\dfrac{ka\omega\mu}{2R}\, e^{-jkR}\, J_1(k_{11}a)\,(1+\cos\Theta)\,\dfrac{J_1'(ka\sin\Theta)}{1-(ka\sin\Theta/k_{11}a)^2}\,\cos\varphi & \text{(A-2)} \end{cases}$$

$$k_{11}a = 1.841 \quad .$$

The feed-horn aperture geometry is shown in Fig. A-1. Since the X- and Y-components are given by

$$\begin{cases} E_{TX} = E_\Theta \cos\varphi \cos\Theta - E_\varphi \sin\varphi \\ E_{TY} = E_\Theta \sin\varphi \cos\Theta + E_\varphi \cos\varphi \end{cases} , \qquad \text{(A-3)}$$

we can write

$$TE_{11} \quad \begin{cases} E_{TX}(\Theta,\varphi) = A\,[F_1(\Theta)\cos\Theta - F_2(\Theta)]\,(1+\cos\Theta)\sin\varphi\cos\varphi \\ E_{TY}(\Theta,\varphi) = A\,[F_1(\Theta)\sin^2\varphi\cos\Theta + F_2(\Theta)\cos^2\varphi]\,(1+\cos\Theta) \end{cases} \qquad \text{(A-4)}$$

where A is a constant as regards the Θ, φ variations and

$$F_1(\Theta) = \frac{J_1(ka\sin\Theta)}{ka\sin\Theta} \quad , \qquad \text{(A-5)}$$

$$F_2(\Theta) = \frac{J_1'(ka\sin\Theta)}{1-(ka\sin\Theta/k_{11}a)^2} \quad . \qquad \text{(A-6)}$$

Since $E_{TX} = 0$ for $\varphi = 0,\ \pi/2$ and $E_{TX} \neq 0$ for $\varphi = \pi/4,\ 3\pi/4$, we call E_{TX} the cross-polarized field component. Similarly, since $E_{TY} \neq 0$ for $\varphi = 0,\ \pi/2$, we call E_{TY} the normally polarized component. Now we change to the Cassegrainian co-ordinates [Fig. A-2(a-b)], noting that $\Theta = \gamma$ and $\varphi \equiv \xi$, and we have finally, for the TE_{11} mode feed-horn patterns,

$$\begin{cases} E_X(\gamma,\xi) = A(1+\cos\gamma)\sin\xi\cos\xi\,[F_1(\gamma)\cos\gamma - F_2(\gamma)] & \text{(A-7)} \\ E_Y(\gamma,\xi) = A(1+\cos\gamma)\,[F_1(\gamma)\cos\gamma\sin^2\xi + F_2(\gamma)\cos^2\xi] & \text{(A-8)} \end{cases}$$

$$F_1(\gamma) = \frac{J_1(ka\sin\gamma)}{ka\sin\gamma} \quad , \qquad \text{(A-9)}$$

$$F_2(\gamma) = \frac{J_1'(ka\sin\gamma)}{1-(ka\sin\gamma/k_{11}a)^2} \quad . \qquad \text{(A-10)}$$

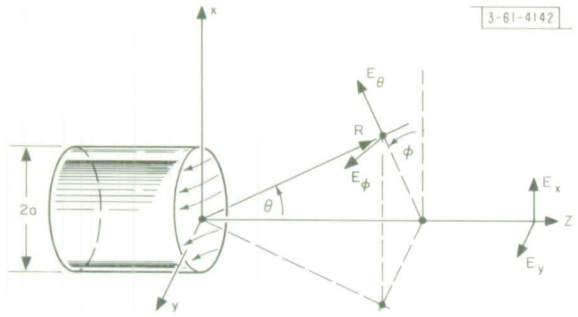

Fig. A-1. Feed-horn geometry.

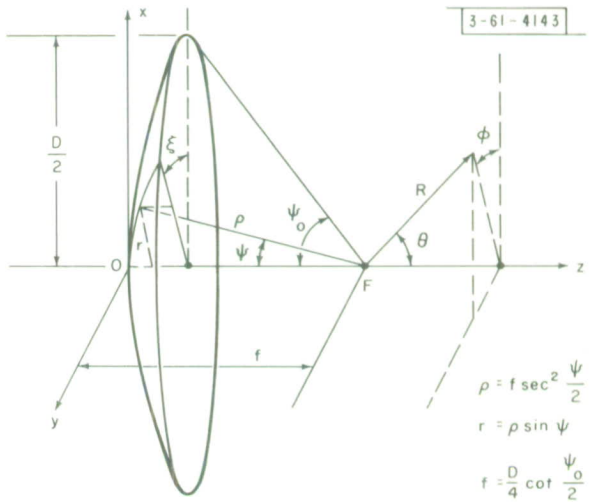

Fig. A-2(a). Paraboloid geometry.

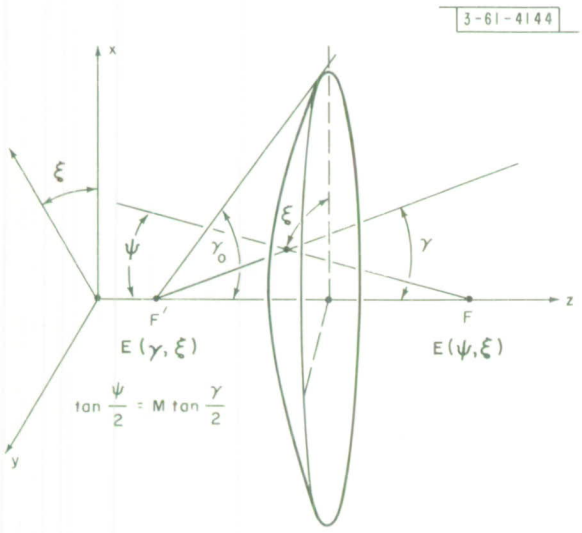

Fig. A-2(b). Hyperboloid geometry.

The radiated field components for the TM_{01} mode are given by[12]

$$\begin{cases} E_{\xi} = 0 & \text{(A-11)} \\ E_{\gamma} = -j \dfrac{ka(k_{01})}{2R} \dfrac{1+\cos\gamma}{\sin\gamma} J'_o(k_{01}a) \dfrac{J_o(ka\sin\gamma)}{1-(k_{01}a/ka\sin\gamma)^2} & \text{(A-12)} \end{cases}$$

$$k_{01}a = 2.405 \quad .$$

By following the preceding procedure, we have

$$TM_{01} \begin{cases} E_{TX}(\gamma,\xi) = B(\dfrac{1+\cos\gamma}{\sin\gamma}) \cos\gamma \cos\xi \dfrac{J_o(ka\sin\gamma)}{1-(k_{01}a/ka\sin\gamma)^2} & \text{(A-13)} \\ E_{TY}(\gamma,\xi) = E_{TX}(\gamma,\xi)(\dfrac{\sin\xi}{\cos\xi}) \quad . & \text{(A-14)} \end{cases}$$

These results are Eqs. (6), (7), and (8) in the text with the E-plane as $\xi = \pi/2$, and the H-plane as $\xi = 0$. We see that there is only one radiated component of the TM_{01} mode which reflects the symmetry of the field distributions. Also of importance is the fact that the radiated TM_{01} field is zero on-axis and rises to a maximum value off-axis. This property makes it possible to use the mode for generating tracking signals.

We now derive the expressions giving the radiated fields of the paraboloidal reflector in terms of the feed-horn field components. From Silver[13] we have

$$E(\Theta,\varphi) = C \int_{o.}^{a} \int_{o}^{2\pi} e_1 \frac{[G(\psi,\xi)]^{1/2}}{\rho} e^{jkr\sin\Theta\cos(\xi-\varphi)} \, r \, dr \, d\xi \qquad \text{(A-15)}$$

The coordinate system is shown in Fig. A-2(a). By means of the equivalent parabola concept, we can relate the feed-horn gain functions $G(\gamma,\xi)$ to the image feed-horn gain functions $G(\psi,\xi)$ by

$$G(\psi,\xi) = G(\gamma,\xi)(\frac{\sin\gamma}{\sin\psi})^2 \quad . \qquad \text{(A-16)}$$

This expression is only a statement of the conservation of energy requirement for incident and reflected ray bundles on the subreflector. Also, we have

$$\frac{[G(\psi,\xi)]^{1/2}}{\rho} \, rd \, rd\xi = [G(\gamma,\xi)]^{1/2} \, 2Mf \tan\frac{\gamma}{2} \, d\gamma \, d\xi \quad ,$$

and also for the phase term

$$kr\sin\Theta\cos(\xi-\varphi) = k(2Mf)\tan\frac{\gamma}{2}\sin\Theta\cos(\xi-\varphi)$$

$$= p\cos(\xi-\varphi) \qquad [\text{Fig. A-2(a,b)}]$$

for

$$p = (\frac{\pi D}{\lambda}\sin\Theta)\cot\frac{\gamma_o}{2}\tan\frac{\gamma}{2} \quad .$$

Now we can write

$$\begin{cases} \varphi = 0 \text{ plane} \quad , \quad E(\Theta) = D \int_o^{\gamma_o} \int_o^{2\pi} E(\gamma, \xi)\, e^{jp\cos\xi} \tan\frac{\gamma}{2}\, d\gamma\, d\xi & \text{(A-17)} \\ \varphi = \frac{\pi}{2} \text{ plane} \quad , \quad E(\Theta) = E \int_o^{\gamma_o} \int_o^{2\pi} E(\gamma,\xi)\, e^{jp\sin\xi} \tan\frac{\gamma}{2}\, d\gamma\, d\xi & \text{(A-18)} \end{cases}$$

If $E(\gamma, \xi)$ can be separated into functions of γ, ξ alone, we could possibly integrate out the ξ-variations. For the TE_{11} and TM_{01} mode feed-horn functions, this can be done, and we get forms that are all special cases of the integral relations[14]

$$\begin{cases} \int_o^{2\pi} e^{ip\cos u} \begin{matrix}\cos\\ \sin\end{matrix} (mu)\, du = \{2\pi i^m J_m(p)\} \begin{matrix}\cos\\ \sin\end{matrix} (m\pi) & \text{(A-19)} \\ \int_o^{2\pi} e^{ip\sin u} \begin{matrix}\cos\\ \sin\end{matrix} (mu)\, du = \{2\pi i^m J_m(p)\} \begin{matrix}\cos\\ \sin\end{matrix} (m\,\frac{3\pi}{2}) \quad . & \text{(A-20)} \end{cases}$$

Applying these formulas, we can finally write for the antenna X- and Y-field components in the E- and H-planes

$$TE_{11} \begin{cases} E_{XE} = E_{XH} = 0 & \text{(A-21)} \\ E_{YE}(\Theta) = A_1 \int_o^{\gamma_o} \left\{ F_1(\gamma)\cos\gamma\, J_1'(p) + F_2(\gamma)\, \frac{J_1(p)}{p} \right\} \sin\gamma\, d\gamma & \text{(A-22)} \\ E_{YH}(\Theta) = A_2 \int_o^{\gamma_o} \left\{ F_1(\gamma)\cos\gamma\, \frac{J_1(p)}{p} + F_2(\gamma)\, J_1'(p) \right\} \sin\gamma\, d\gamma & \text{(A-23)} \end{cases}$$

where $F_1(\gamma)$, $F_2(\gamma)$ and p are as previously given.

$$TM_{01} \left\{ E(\Theta) = A_3 \int_o^{\gamma_o} J_1(p)\, \frac{J_o(ka\sin\gamma)}{1 - (k_{01}a/ka\sin\gamma)^2} \cos\gamma\, d\gamma \quad . \right. \qquad \text{(A-24)}$$

These are the equations given in the text as Eqs. (13), (14), and (15).

The feed-horn gain will be calculated next. The following section is closely related to the analysis of Silver[15]. The gain of the radiating aperture is by definition $G = 4\pi\, p_{max}/p_T$ where

$$P_{max} = \frac{E^2_{max}}{2\eta} \quad , \quad P_T = \frac{1}{2\eta} \int_s \{|E_X|^2 + |E_Y|^2\}\, ds \quad .$$

The quantity η is the free-space impedance and the integration is over the aperture plane s.

Using the TE_{11} mode field components in the aperture plane s, Eqs. (2) and (3), we get

$$G = \frac{2(ka)^2}{(k_{11}a)^2 - 1} \quad , \quad k_{11}a = 1.841$$

$$TE_{11} \quad G = 0.837\,(ka)^2 \quad . \qquad \text{(A-25)}$$

Repeating the procedure for the TM_{01} mode and noting that E_{max} now occurs at an angle $\gamma' \neq 0$, we get finally, for ka = 13.9,

$$TM_{01} \quad G = 0.256\ (ka)^2 \quad . \tag{A-26}$$

Then we have the relations

$$\frac{G_{TE_{11}}}{G_{TM_{01}}} = \frac{0.837}{0.256} = 3.27 \equiv +5.145\ \text{db} \tag{A-27}$$

or the TE_{11} mode pattern peak is about 5 db above the TM_{01} mode pattern peak for a linearly polarized case.

APPENDIX B
ANTENNA EFFICIENCY CALCULATIONS

The Cassegrainian antenna efficiency is calculated on the basis of replacing the Cassegrainian system with an equivalent paraboloidal feed-at-focus system. For the usual center-fed paraboloidal system, Silver[16] gives, for the on-axis electric field intensity,

$$E = \frac{2f}{\lambda R}\left[\frac{\eta P G_f}{2\pi}\right]^{1/2}\left|\int_0^{2\pi}\int_0^{\psi_o} E(\psi,\xi)\tan\frac{\psi}{2}\,d\psi\,d\xi\right| \quad . \tag{B-1}$$

Now the antenna gain is given by

$$G = \frac{E^2/2\eta}{P/4\pi R^2} = 4G_f\left(\frac{D}{\lambda}\right)^2\left(\frac{f}{D}\right)^2\left|\int_0^{2\pi}\int_0^{\psi_o} E(\psi,\xi)\tan\frac{\psi}{2}\,d\psi\,d\xi\right|^2 \tag{B-2}$$

and the antenna efficiency is defined as $\eta = G/(\pi D/\lambda)^2$

or

$$\eta = \frac{4G_f}{\pi^2}\left(\frac{f}{D}\right)^2\left|\int_0^{2\pi}\int_0^{\psi_o} E(\psi,\xi)\tan\frac{\psi}{2}\,d\psi\,d\xi\right|^2 \quad . \tag{B-3}$$

As in Appendix A, we replace the Cassegrainian feed gain function by the image gain function, resulting in the equation

$$\eta = \frac{1}{4\pi^2}\cot^2\frac{\gamma_o}{2}\,(G_f)\left|\int_0^{\gamma_o}\int_0^{2\pi} E(\gamma,\xi)\tan\frac{\gamma}{2}\,d\gamma\,d\xi\right|^2 \tag{B-4}$$

which is Eq. (1) in the text. This equation has been derived with several important assumptions. First, the feed horn is assumed to have a point phase center from which a spherical wave is assumed to radiate as viewed from the subreflector region. Second, the energy intercepted by the subreflector is assumed to be entirely redirected to the paraboloid with no scattering or diffraction effects. These approximations and their effect on the accuracy of Eq. (1) is discussed in the text.

To compute the antenna efficiency for the TM_{01} mode feed-horn excitation, we must modify the previous derivation given for the TE_{11} mode, particularly because the maximum value of the radiated field is now at $\Theta_o \neq 0$. The radiated field components are given by the expressions

$$E(\Theta)_{\left(\substack{\varphi=0\\ \varphi=\pi/2}\right)} = \frac{D\cot(\gamma_o/2)}{2R\lambda}\left[\eta\,\frac{P_T}{2\pi}\right]^{1/2}\int_0^{\gamma_o}\int_0^{2\pi}[G(\gamma,\xi)]^{1/2}\exp\left[js\begin{pmatrix}\cos\xi\\ \sin\xi\end{pmatrix}\right]\tan\frac{\gamma}{2}\,d\gamma\,d\xi \tag{B-5}$$

$$S = \left(\frac{\pi D}{\lambda}\sin\Theta_o\right)\cot\frac{\gamma_o}{2}\tan\frac{\gamma}{2} \quad .$$

Following Eqs. (B-2), (B-3), and (B-4), we can write

$$\eta = \frac{\cot^2(\gamma_o/2)\,G_f}{4\pi^2}\left|\int_0^{\gamma_o}\int_0^{2\pi} E_o(\gamma,\xi)\exp\left[js\begin{pmatrix}\cos\xi\\ \sin\xi\end{pmatrix}\right]\tan\frac{\gamma}{2}\,d\gamma\,d\xi\right|^2 \quad . \tag{B-6}$$

From Eq. (A-13), we have

$$[G(\gamma, \xi)]^{1/2} = E_o(\gamma, \xi) \begin{pmatrix} x \\ y \end{pmatrix} = \frac{(1 + \cos\gamma)}{E(\gamma, \xi)_{max}} \cos\gamma \frac{J_o(u)}{u} \frac{1}{1 - (P/u)^2} \begin{pmatrix} \cos\xi \\ \sin\xi \end{pmatrix} \qquad (B\text{-}7)$$

$$P = 2.405 \quad .$$

Because of the relations Eqs. (A-19) and (A-20), the integrals involving ξ all reduce to the forms

$$\int_o^{2\pi} \exp\left[js \begin{pmatrix} \cos\xi \\ \sin\xi \end{pmatrix}\right] \begin{pmatrix} \cos\xi \\ \sin\xi \end{pmatrix} d\xi = -2\pi j J_1(S)$$

and we have

$$\eta = \cot^2 \frac{\gamma_o}{2} \frac{G_f}{E^2_{max}} \left| \int_o^{\gamma_o} \frac{J_1(S)\, J_o(u)}{1 - (P/u)^2} du \right|^2 \qquad (B\text{-}8)$$

$$E^2_{max} = (1 + \cos\gamma')^2 \cos^2\gamma' \left\{ \frac{J_o(u_o)}{u_o} \frac{1}{1 - (P/u_o)^2} \right\}^2_{max} \quad . \qquad (B\text{-}9)$$

For ka = 13.9, $u_o = 3.0$, we have $\gamma' = 10°$ and

$$(ka)^2 E^2_{max} = G_f = 0.256(ka)^2 \qquad [\text{Eq. (A-26)}] \quad .$$

Finally,

$$\eta = \frac{(1 + \cos\gamma_o)^2}{u_o^2} \left| \int_o^{\gamma_o} \frac{J_1(S)\, J_o(u)}{1 - (P/u)^2} du \right|^2 \quad , \quad P = 2.405 \qquad (B\text{-}10)$$

which is Eq. (12) in the text.

APPENDIX C
BLOCKAGE AND PHASE ERROR CALCULATIONS

The effect of blockage on the antenna gain and side-lobe level is usually analyzed by computing the far-field patterns created by the useful aperture and blocked region and subtracting the fields. This results in a reduced gain and increased side-lobe level relative to the unblocked aperture. Following the analysis of Gray,[17] we have the gain reductions due to the subreflector blockage

$$g_s = 20 \log (1 - 2\delta^2)$$

where

$$\delta = \frac{d}{D} = \frac{22}{180} = 0.122$$

$$g_s = -0.264 \text{ db} \quad .$$

For a boom diameter of W = 1.5 inches and assuming a plane-wave blocked region as in Fig. C-1, we have

$$g_b = 20 \log (1 - 1.55 \frac{W}{D}) \quad .$$

For two sets of booms, W/D = 0.0166 and

$$g_b = -0.226 \text{ db} \quad .$$

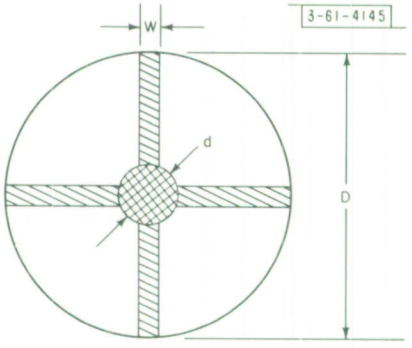

W = 1.5 in.
d = 22 in.
D = 180 in.

Fig. C-1. Blockage shadow region.

The total blockage loss is $g_T = 0.264 + 0.226 = -0.490$ db. It is interesting to compute the entire area blockage weighted in the same manner as the subreflector blockage. We have

$$\frac{d_T}{D} = \frac{\pi(11)^2 + 2(1.5)(180)}{\pi(90)^2} = 0.0362$$

$$g_\ell = -0.654 \text{ db} \quad .$$

This value is, of course, pessimistic, since the illumination is not constant over the boom area.

Since the blockage "field" reduces the main beam peak and increases the side-lobe level, we have for the new side-lobe level, for an assumed −20-db side lobe (Fig. 18),

$$L = 20 \log \left(\frac{0.10 + 0.05\dot{5}5}{1 - 0.0257 - 0.0298}\right)$$

$$L = -15.7\,\text{db} \quad .$$

For an rms phase error of 0.013 inch, we have for the gain loss[18]

$$\frac{G}{G_o} \approx 1 - \bar{\delta}^2$$

where

$$\frac{G}{G_o} = -0.014\,\text{db} \quad .$$

To summarize, the total blockage and phase error gain loss is given below and in the text.

Effect	Calculated Gain Loss (db)
Subreflector blockage	0.264
Boom blockage	0.226
Phase error (0.013 inch rms)	0.014
Total	0.504

APPENDIX D
FEED SYSTEM DRAWING LIST

Part No.	Drawing No.	No. Required	Title
	S-22326		Mechanical Assembly
	C-22324	1	Tracking Feed
	D-19929-6		Conical-Horn Reflector Coordinates
	C-19929-17		Mandrel – Mode Transducer
	C-19929-11		Mandrel – Polarizer
	D-19929-15		Mandrel – Taper
	B-19929-16		Mandrel – Auxiliary Arm
1	C-19929-18	1	Mode Transducer
2	C-19929-10	1	Polarizer
3	B-19929-19	2	1-inch-square i.d. Copper Gasket
4	B-19929-20	1	1-5/16-inch i.d. Copper Gasket
5	S-19929-14	1	Transition Taper
6	D-19946-14	1	Feed Section Plain
7	S-19946-5	1	Conical Horn Reflector
8	D-22326-2	1	Stabilizer
9	C-22326-3	1	Plate
10	D-22326-4	1	Tapered Feed Section
11	C-22326-5	1	Radome Outer
12	C-22326-6	1	Radome Inner
13	A-22326-7	3	Stabilizer Screw
31		1	O-Ring 6-3/4 i.d. × 3/32-inch Wall
32		2	O-Ring 8 i.d. × 1/8-inch Wall
33		1	Shaft Seal (6-1/4-inch-diameter shaft)

ACKNOWLEDGMENTS

The author wishes to acknowledge the assistance and guidance of Mr. L.J. Ricardi during this program. The computations were programmed for the IBM 7094 by Mr. R. J. Peck. Messrs. L. Baghdoyan and A. Sanderson of Group 71 were responsible for the mechanical design of the antenna system and their constant cooperation was appreciated.

REFERENCES

1. J.N. Hines, Tingye Li, and R.H. Turrin, "The Electrical Characteristics of the Conical-Horn Reflector Antenna," Bell System Tech. J. XLII, 1187 (July 1963).
2. B.F. LaPage, "The West Ford Antenna System," Technical Report 338, Lincoln Laboratory, M.I.T. (6 December 1963), DDC 438879.
3. R.N. Assaly, "The Guide Wavelength of Cylindrical Waveguide of Arbitrary Cross Section and a Computer Program for Calculating Values," Technical Report 313, Lincoln Laboratory, M.I.T. (20 May 1963), DDC 412518.
4. A.H. Kessler and W.J. Getsinger, "A Simple Method for Designing an Elliptical Polarizer in Square Waveguide," Group Report 46G-3, Lincoln Laboratory, M.I.T. (28 May 1963), DDC 407624, H-514.
5. J.S. Cook and R. Lowell, "The Autotrack System," Bell System Tech. J. XLII, 1283 (July 1963).
6. P.H. Hannan, "Microwave Antennas Derived from the Cassegrainian Telescope," Trans. IRE, PGAP AP-9, 140 (1961).
7. S. Silver, Microwave Antenna Theory and Design, Radiation Laboratory Series, M.I.T. (McGraw-Hill, New York, 1949), p. 337.
8. A. Dion, "The Aperture Efficiency of Some Horn-Fed Paraboloidal Reflectors," Group Report 61G-3, Lincoln Laboratory, M.I.T. (30 December 1963), DDC 431779, H-566.
9. A. Cohen and A.W. Maltese, "The Lincoln Laboratory Antenna Test Range," Microwave J. 4, No.4, 57 (April 1961).
10. W.V.T. Rusch, "Scattering from a Hyperboloidal Reflector in a Cassegrainian Feed System," Trans. IRE, PGAP AP-11, 414 (1963).
11. S. Silver, op. cit., p. 337.
12. _____, ibid., p. 338.
13. _____, ibid., p. 421.
14. J.A. Stratton, Electromagnetic Theory, (McGraw-Hill, New York, 1941), p. 412.
15. S. Silver, op. cit., pp. 340-341.
16. _____, ibid., p. 424.
17. C.L. Gray, "Estimating the Effect of Feed Support Member Blocking on Antenna Gain and Side-Lobe Level," Microwave J. 7, No.3, 88 (March 1964).
18. H. Jasik, Antenna Engineering Handbook (McGraw-Hill, New York, 1961), pp. 2-40.

DOCUMENT CONTROL DATA – R&D

(Security classification of title, body of abstract and indexing annotation must be entered when the overall report is classified)

1. ORIGINATING ACTIVITY *(Corporate author)*
Lincoln Laboratory, M. I. T.

2a. REPORT SECURITY CLASSIFICATION
Unclassified

2b. GROUP
None

3. REPORT TITLE
Lincoln Experimental Terminal Antenna System

4. DESCRIPTIVE NOTES *(Type of report and inclusive dates)*
Technical Report

5. AUTHOR(S) *(Last name, first name, initial)*
LaPage, Bernard F.

6. REPORT DATE
4 October 1965

7a. TOTAL NO. OF PAGES
60

7b. NO. OF REFS
18

8a. CONTRACT OR GRANT NO.
AF 19(628)-5167

b. PROJECT NO.
649L

c.

d.

9a. ORIGINATOR'S REPORT NUMBER(S)
Technical Report 404

9b. OTHER REPORT NO(S) *(Any other numbers that may be assigned this report)*
ESD-TDR-65-458

10. AVAILABILITY/LIMITATION NOTICES
Distribution of this document is unlimited.

11. SUPPLEMENTARY NOTES
None

12. SPONSORING MILITARY ACTIVITY
Air Force Systems Command, USAF

13. ABSTRACT

The Lincoln Experimental Terminal (LET) is a small transportable ground terminal for testing and evaluating space communications techniques. The requirements, design analysis, and performance data for the LET antenna and feed system are described. The 15-foot-aperture antenna has Cassegrainian optics, and a conical-horn-reflector feed exciter producing opposite-hand circularly polarized transmitting and receiving beams. The simultaneous operation of a two-channel tracking system is also discussed.

14. KEY WORDS

LET
antennas
space communications
Cassegrainian system
conical antennas
horn-reflector antenna